



Cite this: *Green Chem.*, 2022, **24**, 1021

Glyme-based electrolytes: suitable solutions for next-generation lithium batteries

Daniele Di Lecce, ^a Vittorio Marangon, ^{a,b} Hun-Gi Jung, ^c Yoichi Tominaga, ^{d,e} Steve Greenbaum ^f and Jusef Hassoun ^{*a,b,e,g}

The concept of green in a battery involves the chemical nature of electrodes and electrolytes as well as the economic sustainability of the cell. Although these aspects are typically discussed separately, they are deeply interconnected: indeed, a new electrolyte can allow the use of different cathodes with higher energy, lower cost or more pronounced environmental compatibility. In this respect, we focus on an alternative class of electrolyte solutions for lithium batteries formed by dissolving LiX salts in glyme solvents, *i.e.*, organic ethers with the molecular formula $\text{CH}_3\text{O}[\text{CH}_2\text{CH}_2\text{O}]_n\text{CH}_3$ differing by chain length. The advantages of these electrolytes with respect to the state-of-the-art ones are initially illustrated in terms of flammability, stability, toxicity, environmental compatibility, cell performances and economic impact. A particular light is shed on the stability of these systems, particularly in the polymer state, and in various environments including oxygen, sulfur and high-energy lithium metal. Subsequently, the most relevant studies on the chemical–physical features, characteristic structures, favorable properties, and electrochemical behavior of glyme-based solutions are discussed, and the most recent technological achievements in terms of cell design and battery performance are described. In the final sections, the use of glyme-based electrolytes in high-energy cells arranged by coupling a lithium-metal anode with conventional insertion cathodes as well as in alternative and new batteries exploiting the Li–S and Li–O₂ conversion processes is described in detail. The various paragraphs actually reveal the advantages, including safety, low cost and sustainability, which can be achieved by employing the glyme-based electrolytes with respect to the commercially available ones, in particular taking into account future and alternative applications. Particular relevance is given to the glymes with long chains that show remarkable stability, high safety and very low toxicity. Therefore, this review is expected to shed light on the potentialities, the actual advantages compared to the state-of-the-art batteries, and the possible applications of electrolytes based on glyme solvents in next-generation energy storage systems.

Received 27th October 2021,
Accepted 16th December 2021

DOI: 10.1039/d1gc03996b
rsc.li/greenchem



^aGraphene Labs, Istituto Italiano di Tecnologia, via Morego 30, Genova, 16163, Italy.
E-mail: jusef.hassoun@iit.it, jusef.hassoun@unife.it

^bUniversity of Ferrara, Department of Chemical, Pharmaceutical and Agricultural Sciences, Via Fossato di Mortara 17, 44121 Ferrara, Italy

^cCenter for Energy Storage Research, Korea Institute of Science and Technology (KIST), Hwarangno 14-gil 5, Seongbuk-gu, Seoul, 02792, Republic of Korea

^dTokyo University of Agriculture and Technology, Graduate School of Bio-Applications and Systems Engineering (BASE), 2-24-16, Naka-cho, Koganei-shi, Tokyo 184-8588, Japan

^eInstitute of Global Innovation Research (GIR), Tokyo University of Agriculture and Technology, Tokyo, Japan

^fHunter College of CUNY, 695 Park Avenue, NY 10065, New York, USA

^gNational Interuniversity Consortium of Materials Science and Technology (INSTM) University of Ferrara Research Unit, University of Ferrara, Via Fossato di Mortara, 17, 44121 Ferrara, Italy

1. Introduction

Several literature papers proposed improvement of the sustainability of electrochemical energy storage systems focused on the green nature of various cell components. On the other hand, the most significant approach for achieving sustainability and the green concept is the demonstration of actual advances in comparison with the existing technologies.¹ In this respect, the widespread use of lithium-ion (Li-ion) batteries over the past decades has been driving a notable technological change in our society and is currently enabling a gradual transition to a more environmentally sustainable automotive mobility.² Smartphones, laptops, and tablets powered by lithium-ion cells are among the most used devices in our daily life, and hybrid and full electric vehicles are becoming widely adopted, thanks to several programs launched worldwide to decrease environmental pollution.³ Furthermore, Li-ion batteries could play a key role in developing smart grids

coupled with renewable energy sources,⁴ as suggested by the already installed and operating battery packs for stationary storage.⁵ Driven by the undeniable success of the Li-ion technology, ambitious targets have been set by several countries to further boost cell performance by increasing the energy density, and the lithium–metal battery design has been identified as one of the most promising new systems.⁶ Despite a few practical examples of commercial lithium–metal batteries, various challenges still have to be overcome to develop high-energy cells with a suitable safety level and a reliable long-term behavior.⁶ In this regard, the characteristic properties of the most common electrolyte solutions for Li-ion batteries pose some issues.⁷ These solutions typically consist of mixtures of a lithium salt (*e.g.*, LiPF₆) and organic ester solvents, such as alkyl carbonates, and indeed exhibit high conductivity which enable a satisfactory battery performance in terms of capacity, energy density, and rate capability.⁷ On the other hand, these electrolytes are volatile, flammable, and poorly stable when in contact with lithium metal, in particular during prolonged operation.^{8–10} Therefore, several research studies have been focusing since nineties on optimizing alternative electrolyte solutions,^{11–15} such as those prepared by dissolving a lithium salt in a lowly volatile and modestly flammable ether oligomer with a $-(CH_2CH_2O)-$ unit, that is, ethylene oxide (EO)-glymes.^{16–24} EO-based glymes can be synthesized from ethylene epoxide by various large scale methods, including reaction in an alcoholic environment with sodium following the Williamson mechanism, methylation of glycol ether with methyl sulfate, Lewis acid-catalyzed cleavage of ethylene oxide by ether, and reaction of ethylene glycol with alcohol catalyzed polyperfluorosulfonic acid resin at high temperature and pressure.²⁵ Instead, aliphatic carbonates presently used in battery electrolyte formulations may be industrially achieved by more complex organic pathways including phosgenation, oxidative carbonylation, reaction of urea with alcohols, reaction of oxiranes with carbon dioxide, through metal carbonates, and by carbonate interchange reaction.²⁶ In particular, dialkyl carbonates such as DMC and DEC, may be prepared from halohydrins, and from alcohols and carbon monoxide with elemental sulfur, while alicyclic carbonates such as EC may be obtained from the corresponding halogenated carbonates.²⁶ For readers' convenience, Table 1 reports the acronyms of the several chemical species discussed herein.

In addition to the simplest and more environmentally friendly preparation pathway compared to those of the common electrolyte solvents used in batteries (*i.e.*, EC, DMC, EMC, and DEC), glymes, and particularly those with longer chain lengths (G₃, G₄, and PEGDME), are characterized by a more relevant safety content, lower flammability and flash point as well as less relevant toxicity except for possible issues on fertility expected for glymes with lower chain lengths. Table 2 displays the physical–chemical properties of the conventional carbonate solvents and glymes used for battery application, including the related safety hazards as indicated by the SDS data (Sigma-Aldrich) and confirmed by the literature.^{25,27–31} PC and EC are the only carbonate solvents

Table 1 Acronyms of the various compounds and chemical species cited throughout the text

Chemical species	Acronym
<i>n</i> Glyme, <i>n</i> (ethylene glycol) dimethyl ether, CH ₃ -O-(CH ₂ -CH ₂ -O) _{<i>n</i>} -CH ₃	G _{<i>n</i>}
Poly(ethylene glycol) dimethyl ether	PEGDME
Poly(ethylene oxide)	PEO
Poly(methyl methacrylate)	PMMA
Poly(butyl acrylate)	PBA
Polypyrrole	PPy
1,3-Dioxolane	DOL
1,2-Dimethoxy ethane	DME (or G ₁)
Ethylene glycol diethyl ether	EG
Dimethylacetamide	DMA
Tetrahydrofuran	THF
1,1,2,2-Tetrafluoroethyl 2,2,3,3-tetrafluoropropyl ether, hydrofluoroether	HFE
Propylene carbonates	PC
Ethylene carbonates	EC
Dimethyl carbonates	DMC
Methylethylcarbonate, ethylmethylcarbonate	EMC
Diethyl carbonate	DEC
Fluoroethylene carbonate	FEC
Methylethylcarbonate	MEC
Acetonitrile	ACN
Dimethyl sulfoxide	DMSO
Dimethylformamide	DMF
Dimethylacetamide	DMA
Γ-Butyrolactone	GBL
Tetraethylsulfamide	TESA
Lithium-bis-(trifluormethanesulfonyl)-imide, LiN(SO ₂ CF ₃) ₂ , often LiTFSA	LiTFSI
Lithium bis(fluoro sulfonyl)imide, LiN(SO ₂ F) ₂ , often LiFSA	LiFSI
Cyclic imide, lithium 1,2,3-dithiazolidine-4,4,5,5-tetrafluoro-1,1,3,3-tetraoxide, LiN(C ₂ F ₄ S ₂ O ₄)	LiCTFSI
Lithium hexafluorophosphate	LiPF ₆
Lithium tetrafluoroborate	LiBF ₄
Lithium bis(perfluoroethanesulfonyl)imide, often LiBETA	LiBETI
Lithium tetrafluoroborate	LiTFB
Lithium trifluoromethylsulfonate, lithium triflate, LiSO ₃ CF ₃	LiTf
Lithium trifluoroacetate	LiTFA
Lithium 2-trifluoromethyl-4,5-dicyanoimidazole	LiTDA
Lithium tetra(trifluoromethanesulfonyl)propene	LiTFSP
Lithium bis(nonafluorobutanesulfonyl)imide, LiN(C ₄ F ₉ SO ₂) ₂ often LiNFSI	LiNFSI
Lithium nitrate	LiNO ₃
Lithium bis(pentafluoroethylsulfonyl)imide, LiN(SO ₂ C ₂ F ₅) ₂	LiBETI
Lithium bis(oxalato)borate, LiC ₄ BO ₈	LiBOB
Dilithium dodecafluorododecaborate, Li ₂ B ₁₂ F ₁₂	Li ₂ DBF
<i>N,N</i> -Diethyl- <i>N</i> -methyl- <i>N</i> -(2-methoxyethyl) ammonium bis(trifluoromethanesulfonyl)imide	DEMETFSI
Methyl butyl pyrrolidinium-bis-(trifluoromethanesulfonyl)-imide	Pyr ₁₄ TFSI
1,1,2,2-Tetrafluoroethyl 2,2,2-trifluoroethyl ether	TFTFE
LiNi _x Mn _y Co _z O ₂	NMC
Solid electrolyte interphase	SEI
Ionic liquid	IL
Solvate ionic liquid	SIL
Solvent separated ion pair	SSIP
Contact ion pair	CIP
Vinylene carbonate	VC
Vinylethylene carbonate	VEC
1,3-Propane sultone	13PS
Hard carbon	HC
Trimethyl phosphate	TMP
Triethyl phosphate	TEP
Tripropyl phosphate	TPrP

Table 1 (Contd.)

Chemical species	Acronym
2-(2,2,2-Trifluoroethoxy)-1,3,2-dioxaphospholane 2-oxide	TFEP
2,2,2-Trifluoroethyl methyl carbonate	FEMC
Di-(2,2,2-trifluoroethyl)carbonate	DFDEC
1,1,2,2-Tetrafluoroethyl-2',2',2'-trifluoroethyl ether	TTFE
Ethoxy(pentafluoro)cyclotriphosphazene	PFPN
Polystyrene	PS
Poly(ethylene glycol) methacrylate	PEGMA
poly(ethylene glycol) dimethacrylate	PEGDMA
poly(ethylene glycol) methyl ether acrylate	PEGA

without flammability; however EC has an elevated toxicity. Instead, EC and DMC which are typically combined as the electrolyte solvents for LIBs are highly flammable, thus suggesting the need for a safer alternative.³² On the other hand, glymes show a favorable trend associated with the lengthening of the $-\text{CH}_2\text{CH}_2\text{O}-$ chains. Indeed, DME (G_1) and DEGDME (G_2) are the only glyme species to show relevant flammability, while TREGDME (G_3) and TEGDME (G_4) exhibit low toxicity and liquid PEGDMEs (250 and 500 g mol⁻¹) are classified as non-dangerous for humans. Despite DME being usually employed in Li-S batteries due to its enhanced stability towards lithium polysulfide intermediates formed by the conversion electrochemical process, the safety issues related to its relevant volatility and flammability are by now acknowledged, and the search for safer electrolyte solutions to achieve Li-S devices of practical interest is a deeply investigated topic.³³ Moreover, a decrease of the electrolyte flashpoint may be achieved by using non-flammable co-solvents and flame retardant additives, such as phosphorus-containing (e.g., TMP, TEP, TPrP, and TFEP) and fluorinated (e.g., FEMC, FEC, DFDEC, TTFE, and PFPN) species,³⁴ or by functionalization of the glyme solvent.³⁵ Among the various approaches, solid electrolyte configurations may represent a viable strategy to increase the safety content of

the battery due to enhanced chemical, thermal and mechanical stability. Ceramic electrolytes such as garnet-type $\text{Li}_7\text{La}_3\text{Zr}_2\text{O}_{12}$ (LLZO) or NASICON-derived structures, *e.g.*, $\text{Li}_{1.5}\text{Al}_{0.5}\text{Ge}_{1.5}(\text{PO}_4)_3$ (LAGP), provide fast Li^+ transport and suitable ionic conductivity at room temperature, despite the cycling behavior likely to be affected by the interphase stability due to poor contact between the electrodes and electrolyte in the cell.³⁶ On the other hand, solid polymer electrolytes benefit from suitable electrode/electrolyte contact and remarkable conductivity which, however, are reached at medium-high operative temperatures. Indeed, PEO-based electrolytes usually require temperatures above 65 °C to allow proper amorphization of the crystalline structure and satisfactory battery performance,³⁷ which may be improved through the introduction of copolymer blocks such as PS, PEGMA, PEGDMA or PEGA,^{36,38} or ceramic fillers such as SiO_2 , ZrO_2 or TiO_2 in the PEO matrix.^{37,39,40} The substitution of PEO with polycarbonate species was recently considered due to the lower crystallinity and good oxidative stability, even though their low stability towards lithium metal may limit their application.³⁶ Furthermore, alternative polymer chemistries can be employed to stabilize the lithium anode and synthesize effective separators in order to enhance the Li^+ exchange between the electrodes.^{41,42}

Along with the initial conceptualization and pioneering studies of glyme-based electrolytes, Li-metal batteries using the most common intercalation electrodes, such as LiCoO_2 and graphite, as well as other insertion cathodes such as LiFePO_4 , were proposed with promising results, in spite of several issues which were firstly identified.^{43–60} Afterwards, “high-concentration” glyme-based electrolytes have attracted a great deal of attention due to their favorable properties, and there is an intriguing dilemma on the actual nature of these mixtures, which have been described as either solvent-in-salt solutions or solvated ionic liquids (SILs).^{61–82} Moreover, glyme-based electrolytes have been gaining renewed interest due to a

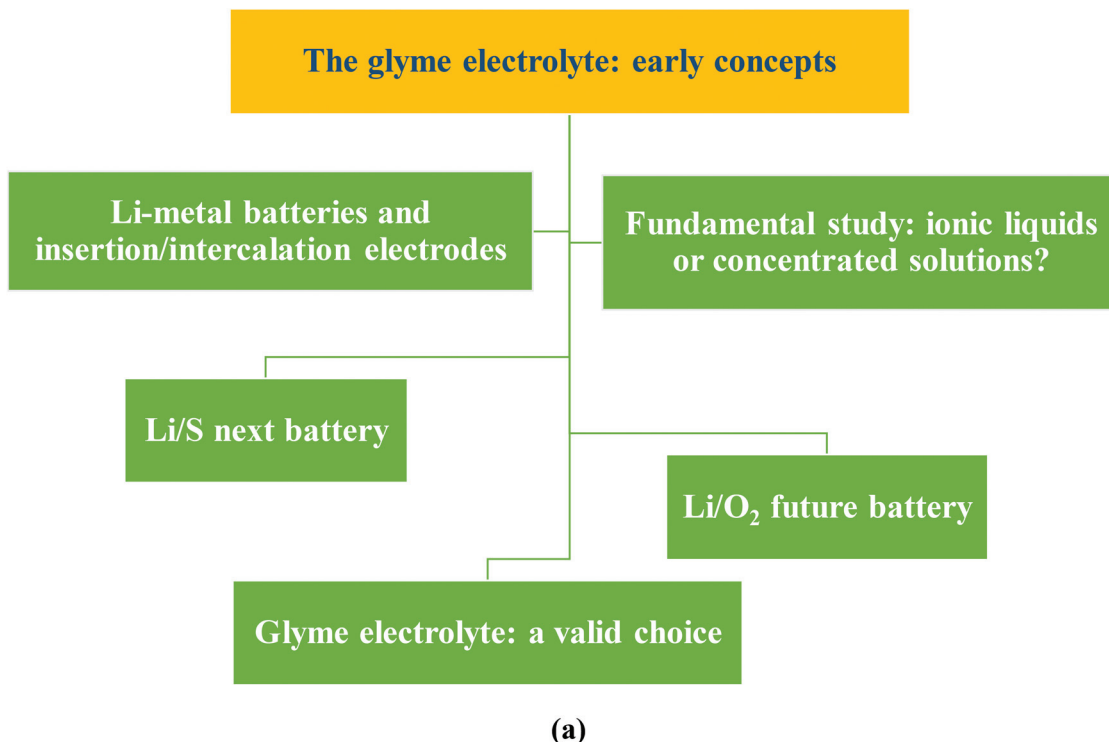
Table 2 Physical-chemical properties of carbonate and glyme solvents employed for battery application. The SDS data are provided by Sigma-Aldrich

Solvents	Safety hazards (SDS)	Melting point [°C]	Boiling point [°C]	Flash point [°C]	Density [g cm ⁻³]	Viscosity [mPa s]
DMC	- Flammable	2	90 (ref. 27)	18 (ref. 27)	1.069	0.59 (ref. 28)
EC	- Elevated toxicity - Irritating	35	248 (ref. 27)	160 (ref. 27)	1.321	2.56 (ref. 28)
PC	- Irritating	-55	242 (ref. 27)	132 (ref. 27)	1.204	2.5 (ref. 28)
EMC	- Flammable	-55	109 (ref. 27)	23 (ref. 27)	1.006	0.65 (ref. 29)
DEC	- Flammable	-43	126 (ref. 27)	33 (ref. 27)	0.975	0.753 (ref. 28)
DME	- Flammable - Irritating - May affect fertility	-58	84 (ref. 27)	-2 (ref. 27)	0.867	0.42–0.46 (ref. 25)
DEGDME	- Flammable - May affect fertility	-64	162	57	0.94	0.98–1.0 (ref. 25)
TREGDME	- Irritating - May affect fertility	-45	225	113	0.985	1.95–2.16 (ref. 25)
TEGDME	- May affect fertility	-30	276 (ref. 27)	140 (ref. 27)	1.009	3.3–3.7 (ref. 25)
PEGDME (250 g mol ⁻¹)	—	-23	240	135	1.03	7.2 (20 °C) (ref. 30)
PEGDME (500 g mol ⁻¹)	—	13	>250	254	1.07	28 (20 °C) (ref. 30)

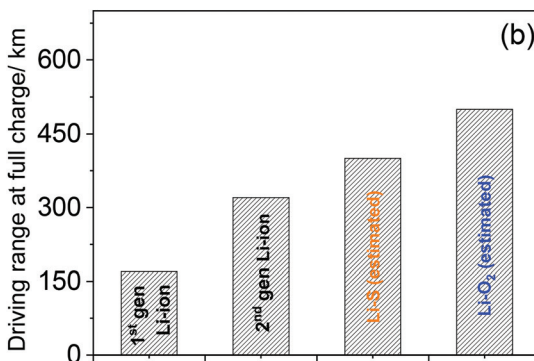


possible suitability for the emerging high-energy lithium-sulfur (Li-S) battery, which is formed by combining a lithium-metal anode and a sulfur-based cathode.^{83–102} This new technology is nowadays considered close to practical applications and holds promise of a breakthrough in storable energy per unit mass.^{103,104} Furthermore, glyme-based solutions have been selected as the electrolytes of choice for the lithium–oxygen (Li–O₂) cell, in which a lithium–metal anode is coupled with a gas diffusion layer electrode enabling O₂ electrochemical conversion thanks to an open design. Notably, this system could store even more energy than the Li-S cell and has been suggested as a possible battery for future applications.^{105–130} In this review, we discuss with chronologi-

cal details various developments in the research on glyme-based electrolytes for lithium batteries, which are summarized in the scheme in Fig. 1 (panel a). For the reader's convenience the various techniques and expressions cited throughout the following sections are listed and explained in Table 3. Furthermore, panel b of Fig. 1 reports a comparison between the present Li-ion battery and the two emerging energy storage systems (*i.e.*, Li-S and Li–O₂ cells), which can allow the use of glyme-based electrolytes for possible application in electric vehicles. The figure suitably reveals the advances potentially achieved by these new systems both in terms of the driving range (km by a single charge)¹³¹ and in terms of the economic impact (USD per kW h of battery pack).¹³²



(a)



(b)

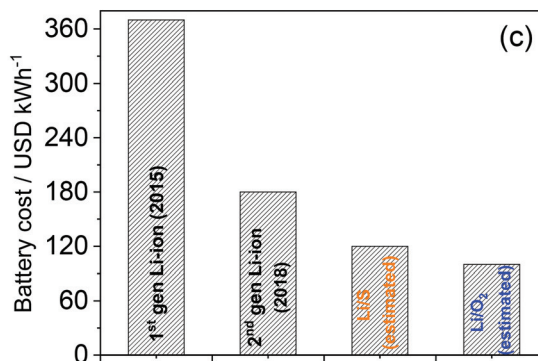


Fig. 1 (a) Schematic of the main research topics involving the fundamental and technological investigations of glyme-based electrolytes for lithium batteries carried out over the past 25 years. (b and c) Comparison between the present Li-ion battery and the two emerging energy storage systems (*i.e.*, Li-S and Li–O₂ cells) which can be allowed by the use of a glyme-based electrolyte for possible application in electric vehicles in terms of (b) the driving range (km by a single charge) and (c) economic impact (USD per kW h of battery pack).



Table 3 Acronyms of the various techniques and expressions cited throughout the text

Techniques and other acronyms	Acronym
Electrochemical quartz crystal microbalance	EQCM-A
Cyclic voltammetry	CV
Electrochemical impedance spectroscopy	EIS
Very-low-frequency electrochemical impedance spectroscopy	VLF-EIS
Galvanostatic cycling	GC
Nuclear magnetic resonance	NMR
Pulse field gradient nuclear magnetic resonance	PFG-NMR
Pulsed-gradient spin-echo nuclear magnetic resonance	PGSE-NMR
Electrophoretic NMR	eNMR
First-principles molecular dynamics	FPMD
Electrochemical mass spectrometry	ECMS
Linear sweep voltammetry	LSV
Solvate ionic liquid	SIL
Contact ion pair	CIP
Scanning electron microscopy	SEM
Transmission electron microscopy	TEM
X-Ray diffraction	XRD
Small-angle X-ray scattering	SAXS
<i>In situ</i> subtractively normalized Fourier transform infrared spectroscopy	SNIFTIRS
X-ray photoelectron spectroscopy	XPS
Thermogravimetric analysis	TGA
Open circuit voltage	OCV
Gas diffusion layer	GDL
Oxygen reduction reaction	ORR
Oxygen evolution reaction	OER
Rotating ring disk electrode	RRDE
Mass spectrometry	MS
High-energy X-ray total scattering	HEXTS
Molecular dynamics	MD
Molecular weight	MW
Molecular orbital	MO
Density functional theory	DFT
Potentials of mean force	PMF
Infrared	IR
X-ray absorption spectroscopy	XAS
X-ray absorption near edge structure	XANES
Oxygen reduction reaction	ORR
Oxygen evolution reaction	OER
Donor number	DN
Highest occupied molecular orbital	HOMO
Lowest unoccupied molecular orbital	LUMO

2. The “glyme electrolyte”: initial studies and fundamental concepts

Pioneering studies on the possible energy-storage applications of glymes were carried out in the late 1990s, mostly driven by encouraging results on the lithium–metal polymer battery employing PEO.⁶ Indeed, electrolytes using low-molecular-weight glymes exhibited promising characteristics in terms of chemical stability and viscosity, thereby holding the promise of an enhanced safety level as compared to that of conventional alkyl-carbonate-based solutions, along with suitable Li⁺ transport properties at room temperature.^{19,53,86} On the other hand, understanding the complex Li-electrode/electrolyte interface in glyme-based cells required several studies, which are still ongoing to fully clarify the characteristic features of such an intriguing and intrinsically safe system. Initial works opened a debate on the actual suitability of this class of elec-

trolyte solutions in high-energy batteries owing to doubtful results on the compatibility of glyme solvents with lithium metal. Accordingly, a first comparative investigation of the Li electrode in solutions of various salts, that is, LiAsF₆, LiClO₄, LiTf, LiTFSI, LiBF₄, LiBr and LiI, in DME, EG, and G₁ solvents, with DOL, PC, EC and DMC as co-solvents, suggested poor surface chemistry and a rough morphology of the metal electrode after electrodeposition–dissolution, which lead to a low cycling efficiency in rechargeable batteries. In this regard, cyclic voltammetry provided insights into the surface films deposited in the cell, as shown in Fig. 2a, which reports a steady-state profile of a polycrystalline gold electrode in solutions using the above-mentioned solvents and LiTf as salt. Li underpotential deposition (UPD) and stripping are marked in the figure along with the non-Faradaic region.¹⁶ However, other studies demonstrated promising characteristics of glyme-based solutions of LiTFSI (G_n with n from 1 to 4), revealing for this salt high compatibility with various solvents and high electrochemical stability. Notably, LiTFSI appeared strongly associated in glymes and moderately associated in TESA at low concentrations, formed stable solvates in G₁ at intermediate concentrations, and displayed thermodynamic properties approaching those of molten salts at high concentrations. Fig. 2b shows the trend of specific conductivity as a function of the concentration of LiTFSI in G_n solvents. Reasonably high specific conductivity was observed for both LiTFSI and LiClO₄ in various solvents, which indicated that the ionic conductance at high concentration in solvents of low dielectric constant was limited by a charge transfer process rather than by the migration of free ions.¹⁷ To verify the hypothesis of stable solvates that persist in the solution influencing its properties, phase diagrams and Raman spectra have been measured for mixtures of LiTFSI and ACN, PC or glymes (G_n, with n = 1, 4, and 10). In fact, the systems without solvates show relative intensities of the solvent and salt Raman bands which are proportional to the concentration. On the other hand, important changes in the relative intensities of these bands reflect the presence of stable solvates in the electrolyte, which are additionally detected in the phase diagrams. Moreover, X-ray crystallography reveals free ions, SSIPs and CIPs in the solutions, suggesting that no stable solvates are formed in (G_n)_x:LiTFSI electrolytes for n > 2.¹⁸ The interplay between the lithium-ion solvation state, ionic conductivity, and charge–discharge cycling efficiency of the Li–metal anode was further investigated. In particular, a ternary mixed solvent consisting of G_n (n from 1 to 4), EC, and EMC, dissolving LiPF₆ (1 M), was comparatively studied. These glyme solutions exhibited higher conductivity and higher lithium cycling efficiency than EC/EMC, while both the conductivity and viscosity typically increased as the ethylene-oxide chain length decreased (decrease in n). Notably, this decrease in viscosity was associated with a change in the lithium-ion solvation structure, which occurred when a glyme was added to EC/EMC and was caused by a selective solvation of the glyme with respect to lithium ions as demonstrated by ¹³C-NMR measurements. The lithium cycling efficiency value depended on the charge-dis-



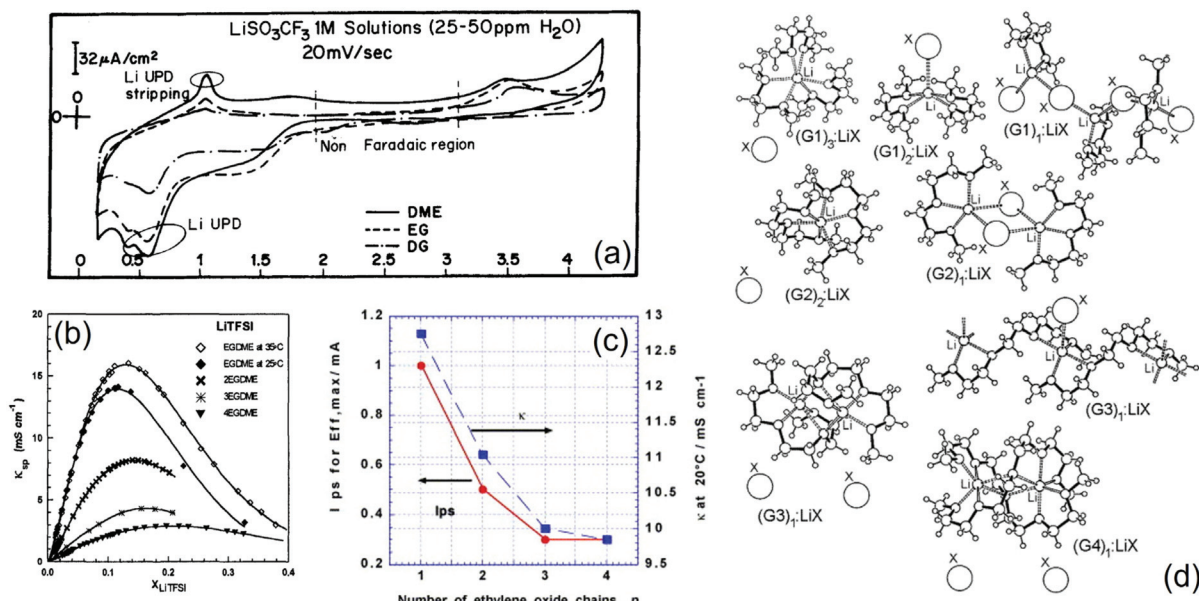


Fig. 2 (a) Typical steady-state voltammograms obtained from polycrystalline gold electrodes in 1 M LiTf solutions of G1 (DME), ethyl glyme (EG) and G₂ (DG). Scan rate: 20 mV s⁻¹. Li underpotential deposition and stripping peaks and the non-Faradaic region are marked. Reproduced with permission.¹⁶ Copyright © 1996 Elsevier Science Ltd. (b) Specific conductivity (κ) at 25 °C of LiTFSI in glymes, that is, DME (EGDME; κ at 35 °C is also shown), G₂ (2EGDME), G₃ (3EGDME), and G₄ (4EGDME). Reproduced with permission.¹⁷ Copyright © 1998 Plenum Publishing Corporation. (c) Relationship between electrolyte conductivity (κ) and charge-discharge cycling current (I_{ps}) for the maximum value of cycling efficiency of lithium (Eff_{max}) and n for 1 M LiPF₆–EM₈₀/ n G₂₀, where EM₁₀₀– x /nG_x represents the mixed solvent of EC/MEC (3 : 7) and n -glyme (mixing volume ratio = 100 – x : x), with plating charge (Q_p) of 0.025 mA h. Reproduced with permission.¹⁹ Copyright © 2003 Elsevier Ltd. All rights reserved. (d) Schematic illustrations of various glyme–LiX solvate structures with G₁, G₂, G₃, and G₄. Reproduced with permission.²¹ Copyright © 2006 American Chemical Society.

charge current (I_{ps}), and the ethylene-oxide number, n , affected this trend. In particular, when n increased there was a decrease in the I_{ps} exhibiting the maximum value of efficiency (Eff_{max}, see Fig. 2c). A similar change in conductivity with n was observed (see Fig. 2c). Among the various glymes taken into account, G₂ or G₃ exhibited very promising characteristics, namely high conductivity and suitable charge-discharge cycling behavior at a high current.¹⁹ In a subsequent report,²⁰ the crystal structures of glyme solvates with LiTFSI and LiBETI were determined, and order-disorder solid phase transitions in many of the solvates were identified. Further work was carried out to shed light on the molecular interactions in glyme-based solutions. Accordingly, phase diagrams of mixtures of G_n (n = 1, 2, 3, and 4) and LiBETI, LiAsF₆, LiI, LiLO₄, LiBF₄, LiTf, LiBr, LiNO₃, and LiCF₃CO₂ were proposed, and the relationships between the ionic association strength of the salt (that is, anion characteristics), chain length of the glyme, solvate formation, and thermophysical properties of the mixture were investigated, thereby providing a comprehensive model of solvate formation and ionic interactions in these electrolyte systems. Fig. 2d illustrates an approximate ordering for increasing the ionic association strength of LiX salts in glymes.²¹ Glymes were suggested to form solid complexes with lithium salts, which would be suitable as “soft” solid electrolytes for Li batteries exhibiting a wide range of ion transport properties. Thus, complexes between LiAsF₆ and G_n (n = 3 and

4) showed significantly different cation transference numbers, resulting from the presence of channels for Li⁺ migration in G₃ and from weak binding of AsF₆⁻ in the structure of G₄.²² Considerable efforts were devoted to understanding the ion-solvent arrangements in the glyme-based electrolyte solutions. For instance, ¹⁹F NMR spectroscopy and conductivity data were collected to determine the ion pair formation constants of LiTFSI and LiTf solutions in mixtures of DOL and G₁, G₂, or water, and the obtained results were interestingly similar to those of liquid PEGDME and solid PEO.²³ Furthermore, the formation constants of ionic pair solutions of lithium salts in G₁, G₂, and G₃ were estimated using ⁷Li, ¹¹B and ¹⁹F NMR analyses, which demonstrated that even in solvents with very similar coordination (in terms of the donor and acceptor number values) and dielectric properties, the ionic pair formation constant depended on effects related to ion agglomerate formation, non-covalent interactions between ions and the liquid matrix, as well as the number of interacting centers in the solvent molecules.²⁴

Therefore, glymes are proposed for LIBs because of the promising features of PEO-based electrolytes, with a stability depending on the specific glyme–salt (G–S) combination. In particular, the salt concentration appears to remarkably influence the electrolyte characteristics in terms of the solvation ability, dissociation degree, and ionic conductivity. The formation of stable G–S solvates is hypothesized and prelimina-



rily verified for specific compositions, while it is excluded for others. Furthermore, the Li/electrolyte interphase characteristics and the charge/discharge efficiency apparently depend on the adopted G-S combination, due to the effects of the electrolyte viscosity and the structure of the ion-solvent species. Possibly, the better efficiency is ascribed to electrolytes formed by using glymes with increased chain lengths (*i.e.*, with increasing n in G_n). In addition, phases with order-disorder structures are observed in some S-G solvates and suggested to affect the ion association degree of the salts, thus modifying the performance of the electrolyte in lithium cells.

3. Li-Metal batteries using "glyme electrolytes" and insertion/intercalation electrodes

Glyme-based electrolytes have shown promising performances in lithium–metal batteries using insertion cathodes. A Li|LiCoO₂ cell employing the [Li(G₄)][CTFSI] complex was assembled and tested, revealing a stable galvanostatic response during 50 cycles. LiCTFSI may form solid and liquid complexes with G₃ and G₄, respectively. Notably, the electrolyte was stable in a wide potential range from 0 to 4.5 V *vs.* Li/Li⁺ and had a much higher thermal stability as compared to that of pure G₄, whilst the vapor pressure of [Li(G₄)][CTFSI] was negligible at temperatures lower than 100 °C. Furthermore, the [Li(G₄)][CTFSI] complex exhibited an ionic conductivity of 0.8 mS cm⁻¹ at 30 °C, which was slightly lower than that of conventional alkyl-carbonate-based electrolyte solutions and higher than that of the [Li(G₃)][CTFSI] complex (see Fig. 3a), in spite of a relatively high viscosity due to the high molar concentration (*ca.* 3 mol dm⁻³). The pulsed gradient spin-echo NMR (PGSE-NMR) method was employed to measure the self-diffusion coefficients of Li⁺ cations, CTFSI⁻ anions, and glyme molecules, and the ionicity (dissociativity) of [Li(G₄)][CTFSI] at 30 °C was estimated to be *ca.* 0.5.⁴³ Another example showed that increasing the amount of glyme in G₄-LiTFSI complexes (where the molar ratio of G₄ ranged from 40 mol% to 60 mol%) decreases the viscosity and increases the ionic conductivity, thereby improving the rate capability of Li|LiCoO₂ cells. In addition, Li|graphite cells with SEI forming additives, such as VC, VEC, and 13PS, showed a cycling performance comparable to that of conventional carbonate-based electrolytes. Lithium cells using Li₄Ti₅O₁₂ and LiFePO₄ along with the [Li(G₄)][TFSI] complex exhibited excellent reversibility due to an optimal working voltage range.⁴⁴ Besides, an electrolyte formed by G₃ and LiFSI in a 1 : 1 molar ratio showed relatively high thermal stability and stable cycling using LiFePO₄ and graphite electrodes, with 82% of capacity retention at 100 cycles.⁴⁵

A literature work suggested that the oxidative stability of glyme molecules can be enhanced by complex formation with alkali metal cations, such as [Li(G_n)₁][TFSI] with $n = 3$ and 4, which were classified as a room-temperature SILs consisting of

a [Li(G_n)₁]⁺ complex cation and a TFSI⁻ anion due to their liquid state maintained over a wide temperature range and a high self-dissociativity (ionicity) at room temperature. The increase in salt concentration in the [Li(G_n)₁][TFSI] equimolar SIL remarkably enhanced the oxidative stability of the solution to a potential as high as 5 V *vs.* Li⁺/Li, likely owing to the donation of lone pairs of ether oxygen atoms to the Li⁺ cation, which resulted in the lowering of the HOMO of the glyme as suggested by *ab initio* molecular orbital calculations. On the other hand, [Li(G_n)_x][TFSI] solutions with $x > 1$ were stable up to 4 V *vs.* Li⁺/Li⁺ (see Fig. 3b and c). NMR data indicated Li⁺ transport in the equimolar complex *via* migration of the [Li(G₃)₁]⁺ solvate, although the ligand exchange mechanism occurred as a result of the electrochemical reaction at the electrode/electrolyte interface in the Li|[Li(G₃)₁][TFSI]|LiCoO₂ cell. This battery exhibited a steady behavior for more than 200 charge–discharge cycles with a voltage range of 3.0–4.2 V.⁴⁶ Further studies of the Li|LiCoO₂ cell using molten [Li(G_n)₁][TFSI] equimolar complexes were carried out to elucidate the relationship between the Li⁺ limiting current density under one-dimensional finite-diffusion conditions and the rate capability. Voltage drops and incomplete discharge of the cell were observed when the applied current was higher than the limiting current density, which may reflect a depletion of the lithium salt in proximity to the cathode or saturation at the anode interphase. Comparative tests of single-particle LiCoO₂ and an electrode sheet in a typical electrolyte solution based on PC, in a binary LiTFSI-(DEME)TFSI ionic liquid, and in a [Li(G_n)₁][TFSI] molten complex suggested that the Li⁺ transport in the solution controls the rate capability of the cells using the latter electrode.⁴⁷ Notably, the [Li(G₃)][TFSI] complex demonstrated a very promising performance in lithium–metal cells using LiFePO₄ and LiNi_{1/3}Mn_{1/3}Co_{1/3}O₂ cathodes. The battery using the former positive electrode operated at about 3 V (Fig. 3d), delivering a rather stable capacity over 600 charge–discharge cycles (Fig. 3g), whilst that using the latter had a working voltage of about 4 V (Fig. 3e) and exhibited a cycling trend strongly depending on the upper voltage cutoff (Fig. 3h). Accordingly, the cell charged up to 4.2 V showed a capacity retention approaching 60% after 400 cycles. Further tests revealed the formation of a favorable Li/electrolyte interphase, thereby suggesting the possible applicability of this electrolyte formulation in lithium batteries.⁴⁸ In this regard, EQCM-A was effectively employed to measure the product of the viscosity (ηL) and density (ρL) of the electrolyte near the electrode surface, *i.e.*, $\eta L \rho L$, along with changes in mass. The collected data showed a decrease in the $\eta L \rho L$ value during lithium deposition and a sharp increase during lithium dissolution, which were ascribed to changes in the concentration and dissolved state of Li⁺ in proximity to the electrode. The latter increase with the Li dissolution may adversely affect the cation transference number, leading to a decrease in the anodic current in the battery.⁴⁹ Highly concentrated electrolytes have been extensively investigated due to their suitable properties for use in lithium metal cells with insertion cathodes. A comparative study of molten mixtures of LiTFSI and



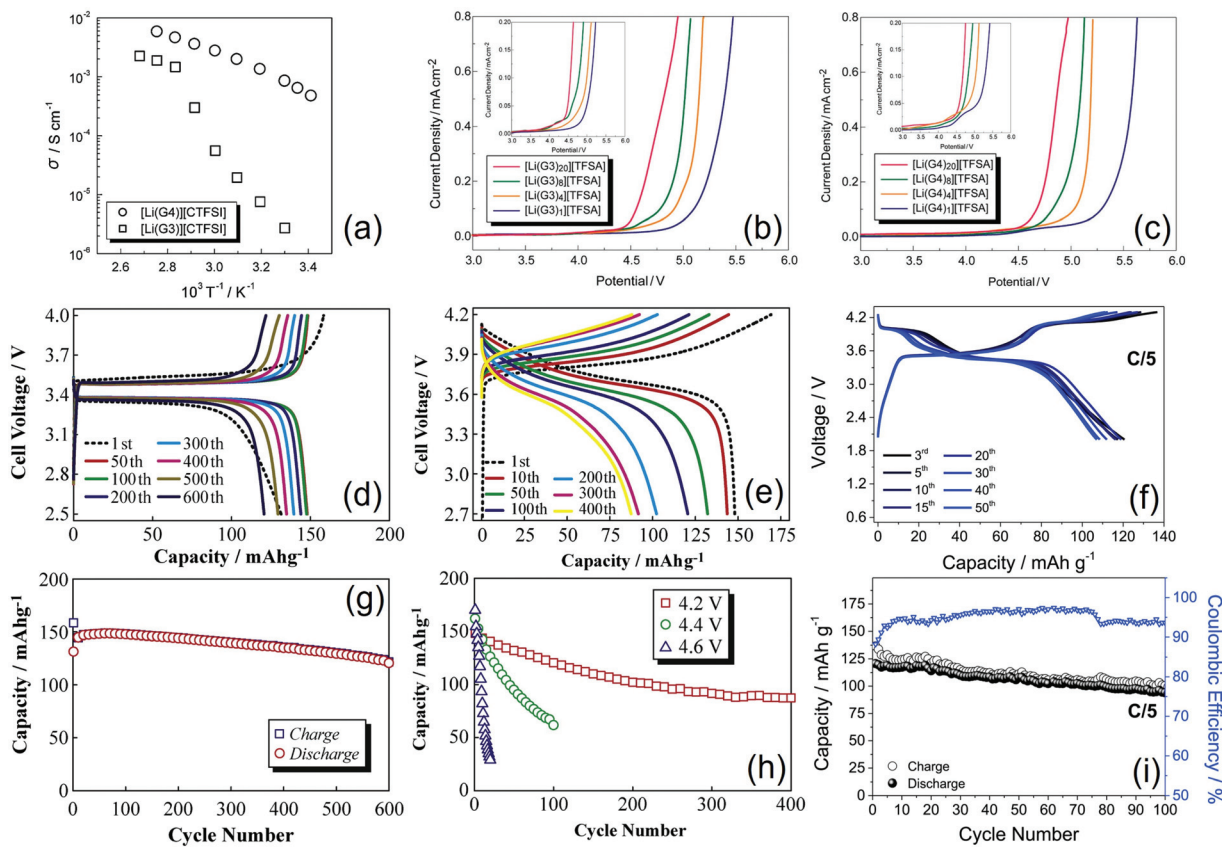


Fig. 3 (a) Temperature dependence of the ionic conductivity of $[\text{Li}(\text{G}_3)]\text{[TFSI]}$ and $[\text{Li}(\text{G}_4)]\text{[TFSI]}$ glyme–Li salt complexes. Reproduced with permission.⁴³ Copyright © 2009 Elsevier B.V. All rights reserved. (b and c) Linear sweep voltammograms of $[\text{Li}(\text{glyme})_x]\text{[TFSI]}$ complexes ($x = 1, 4, 8$, and 20) at a scan rate of 1 mV s^{-1} at 30°C , where the glyme is (b) G_3 and (c) G_4 . Each inset depicts a magnification of current density. Adapted with permission (<https://pubs.acs.org/doi/10.1021/ja203983r>).⁴⁶ Copyright © 2011 American Chemical Society. Further permission related to the material excerpted should be directed to the American Chemical Society. (d and g) Electrochemical behavior of a $\text{Li}|\text{G}_3\text{--LiTFSI}||\text{LiFePO}_4$ cell in terms of (d) voltage profiles at the 1st, 50th, 100th, 200th, 300th, 400th, 500th, and 600th cycle and (g) trend of charge and discharge capacities per positive electrode as a function of the cycle number; temperature: 30°C ; voltage range: $2.5\text{--}4.0 \text{ V}$; and current rate: C/8. (e and h) Electrochemical behavior of a $\text{Li}|\text{G}_3\text{--LiTFSI}||\text{LiNi}_{1/3}\text{Mn}_{1/3}\text{Co}_{1/3}\text{O}_2$ cell in terms of (e) voltage profiles at the 1st, 10th, 50th, 100th, 200th, 300th, and 400th cycle (voltage range: $2.7\text{--}4.2 \text{ V}$) and (h) trend of discharge capacity per positive electrode as a function of the cycle number for various upper charge cutoff voltages (4.2 V, 4.4 V, and 4.6 V); temperature: 30°C ; current: C/8. Adapted with permission.⁴⁸ Copyright © 2013 The Authors. Published by Elsevier B.V. CC BY-NC-ND license. (f and i) Electrochemical behavior of the $\text{Li}|\text{LiTf--LiNO}_3\text{--G}_4|\text{LiMn}_{0.5}\text{Fe}_{0.5}\text{PO}_4$ cell in terms of (f) voltage profiles and (i) trend of charge and discharge capacities per positive electrode and coulombic efficiency as a function of the cycle number; temperature: 25°C ; voltage range: $2.0\text{--}4.3 \text{ V}$; and current rate: C/5 rate ($1\text{C} = 170 \text{ mA g}^{-1}$ with reference to the cathode mass); test performed after an electrochemical activation of the cell. Reproduced with permission.⁵³ Copyright © 2016 Elsevier B.V. All rights reserved.

various ether solvents (THF, G_1 , G_2 and G_3), where the ratio of ether–oxygen atoms to Li^+ (*i.e.*, O/Li) was fixed at four, revealed that the capacity of the $\text{Li}|\text{LiCoO}_2$ cell with $[\text{Li}(\text{THF})_4]\text{[TFSI]}$ dramatically decreased during cycling, whereas a similar cell employing $[\text{Li}(\text{G}_3)_4]\text{[TFSI]}$ displayed a stable behavior with a coulombic efficiency higher than 99% over 100 cycles. These results were related to the oxidative decomposition of the solvents and a persistent Al corrosion occurring in $[\text{Li}(\text{THF})_4]\text{[TFSI]}$ and $[\text{Li}(\text{G}_1)_4]\text{[TFSI]}$, which contain shorter ethers, whilst the use of $[\text{Li}(\text{G}_3)_4]\text{[TFSI]}$ ensured effective suppression of the side reactions.⁵⁰ The literature also suggested that the ionic conductivity of glyme–LiTFSI solvate ionic liquids (SILs) may be inversely proportional to the viscosity, in agreement with Walden's rule. Thus, a decrease in ionic conductivity with increasing concentration of LiTFSI was observed

and associated with the formation of a bulky lithium species, *i.e.*, $[\text{Li}(\text{TFSI})_2]^-$.⁵¹ The $[\text{Li}(\text{G}_4)]\text{[TFSI]}$ complex was employed in a quasi-solid-state electrolyte with fumed silica nanoparticles. This electrolyte was used in double-layered and triple-layered high-voltage bipolar stacked batteries, which showed a working voltage of 6.7 and 10.0 V, respectively, that is, two and three times that of the single-layered device (3.4 V). The double-layered device showed a capacity retention of 99% after 200 cycles at C/2.⁵²

The characteristic features of the positive electrodes have crucial effects on the cell performance as they may influence the working voltage, the properties of the electrode/electrolyte interphase, and the rate capability. Accordingly, an electrolyte formed by dissolving 1 mol LiTf and 1 mol LiNO₃ in 1 kg of G_4 exhibited different behaviors in lithium–metal cells employing



LiFePO₄ and LiMn_{0.5}Fe_{0.5}PO₄ cathodes. The cell using LiFePO₄ operated at 3.5 V with the capacity ranging from 150 mA h g⁻¹ at C/10 to 110 mA h g⁻¹ at 2C, while the one employing LiMn_{0.5}Fe_{0.5}PO₄ showed two plateaus at 4.1 V and 3.5 V (Fig. 3f) with the capacity ranging from 160 mA h g⁻¹ at C/10 to 75 mA h g⁻¹ at 2C, and a stable value of about 125 mA h g⁻¹ for 100 cycles at C/5 (Fig. 3i), where both the specific capacity and current rate were with reference to the mass of the cathode. Notably, the higher working voltage of LiMn_{0.5}Fe_{0.5}PO₄ as compared to that of LiFePO₄ may have a detrimental effect on the coulombic efficiency of the battery.⁵³

We remark that the presence of LiNO₃ in the formulation significantly affects the stability of the electrode/electrolyte interface, as demonstrated in two consecutive studies.^{54,55} Indeed, the cycle life of Li|LiFePO₄ cells with PEGDME (MW 500 g mol⁻¹) dissolving LiTf was significantly enhanced by the addition of LiNO₃ to the electrolyte solution, leading to a stable performance over 60 cycles with a capacity with reference to the cathode of 150 mA h g⁻¹ and a flat working voltage of 3.5 V, which were reflected as a theoretical energy density of 520 W h kg⁻¹ (normalized to the mass of the positive electrode). Furthermore, PFG-NMR measurements suggested suitable ionic conductivity, lithium transference number, ionic-association degree, and self-diffusion coefficient for energy-storage application. It is worth mentioning that the high thermal stability of this electrolyte may remarkably improve the safety of the lithium–metal battery.⁵⁴ In agreement with the above described results, a G₃-LiTf solution was upgraded by adding LiNO₃, which enhanced the electrode/electrolyte interface and widened the electrochemical stability window of the solution, thus enabling its application in a battery with the LiFePO₄ cathode. An electrochemical activation procedure of this cell leading to the formation of stable interfaces at the electrode surface was optimized and thoroughly investigated. Fig. 4 shows the related voltage profiles (a) and the corresponding SEM images of the LiFePO₄/electrolyte interphase upon cycling (b).⁵⁵ Unsymmetrical glymes having different end groups were also studied (Fig. 4c). These glymes had ethyl and butyl end groups and were used to prepare liquid solvates with LiTFSI and LiFSI (glyme : salt ratios of 1 : 1, 2 : 1, and 3 : 1), which exhibited high ionic conductivity at room temperature (on the order of 10⁻³ S cm⁻¹), were stable up to 4.5 V, and ensured a steady galvanostatic performance with LiFePO₄, with a capacity of 145 mA h g⁻¹ (with reference to the cathode) and good rate capability up to 2C at room temperature. Furthermore, preliminary cycling tests with NMC suggested possible applicability in high-voltage batteries and DSC studies indicated a low crystallization temperature between -60 °C and -75 °C for the LiFSI-based electrolyte.⁵⁶ Therefore, both the salt and the glyme chain length may substantially affect the ion transport, the lithium/electrolyte interphase characteristics, and the electrochemical stability window, thereby determining the lithium cell response. Indeed, solutions of LiFSI, LiTFSI, or LiBETI in G_n (n = 2 and 3) had different properties depending on the selected formulation. Thus, decreasing the chain length increased the ionic conduction

tivity from *ca.* 10⁻³ to *ca.* 10⁻² S cm⁻¹, despite having detrimental effects on the lithium transference number. Galvanostatic lithium stripping-deposition and EIS measurements (Fig. 4d–i) suggested that all the electrolytes may form an interphase at the metal anode suitable for a few charge/discharge cycles, with low values of polarization and rather constant resistance values. However, the use of LiBETI led to poor lithium-passivation properties over long-term cycling, whilst widening the anodic stability window to 4.6 V *vs.* Li⁺/Li. Among these various formulations, LiTFSI-based electrolytes were the most adequate for application in Li|LiFePO₄ batteries that ensured a capacity between 134 and 144 mA h g⁻¹ in galvanostatic tests with over 100 cycles at a C/3 rate (1C was 170 mA g⁻¹; both the capacity and C-rate were with reference to the mass of LiFePO₄ in the cathode).⁵⁷ The electrochemical performance of the Li|LiFePO₄ battery was further enhanced as described above, by adding LiNO₃ to these solutions. A thorough investigation of such improved solutions showed evidence of fast ion transport, a wide stability window, suitable lithium–metal passivation, and cathode/electrolyte interphase characteristics that depended on the G_n chain length (n = 2 and 3). An optimized Li|LiFePO₄ battery using a G₃-LiTFSI-LiNO₃ electrolyte delivered 154 mA h g⁻¹ at C/3 without any decay after 200 cycles, as well as a retention above 70% after 500 cycles at 1C and 5C with a coulombic efficiency approaching 100% (Fig. 4j), which benefitted from a stable, ionically conductive electrode/electrolyte interphase (Fig. 4k–n).⁵⁹ Relevantly, a solid composite-electrolyte based on PEGDME (MW 2000 g mol⁻¹), dissolving LiTFSI and LiNO₃, and incorporating nanometric silica (SiO₂) particles was prepared by solvent casting and investigated in Li|LiFePO₄ polymer batteries. This electrolyte had an ionic conductivity higher than 10⁻⁴ S cm⁻¹ at temperatures above 40 °C after subsequent heating and cooling cycles, exhibited a lithium transference number ranging from 0.22 at 45 °C to 0.27 at 70 °C and a low resistance at the interphase with lithium metal, and was stable up to *ca.* 4.4 V. When used in the Li|LiFePO₄ battery at 50 °C, this composite electrolyte enabled a coulombic efficiency of about 100%, a capacity retention approaching 99% after 300 cycles at a C/3 rate, and a maximum capacity of 150 mA h g⁻¹.⁵⁸ Furthermore, G₂ and G₃ dissolving LiTFSI and LiNO₃ in concentrations approaching the solvent saturation limit were used in lithium cells employing the LiFePO₄ cathode, which exhibited a promising cycling performance. Notably, an additional reduction step at a low voltage cutoff (*i.e.*, 1.2 V) during the first discharge allowed the formation of a suitable SEI, as mentioned above (see Fig. 4a and b), thereby leading to a coulombic efficiency of *ca.* 100%, a capacity approaching 160 mA h g⁻¹, and low capacity fading over cycling.⁶⁰

We can reasonably evaluate the glyme-based electrolytes (in particular using G₃ and G₄ and PEGDME) as possible electrolyte solvents for lithium battery application, since they can have a stable electrode/electrolyte interphase, particularly when *ad hoc* additives are used, low volatility, and sufficient dissociation degree. In particular, efficient operation is observed with typical electrodes used in batteries such as



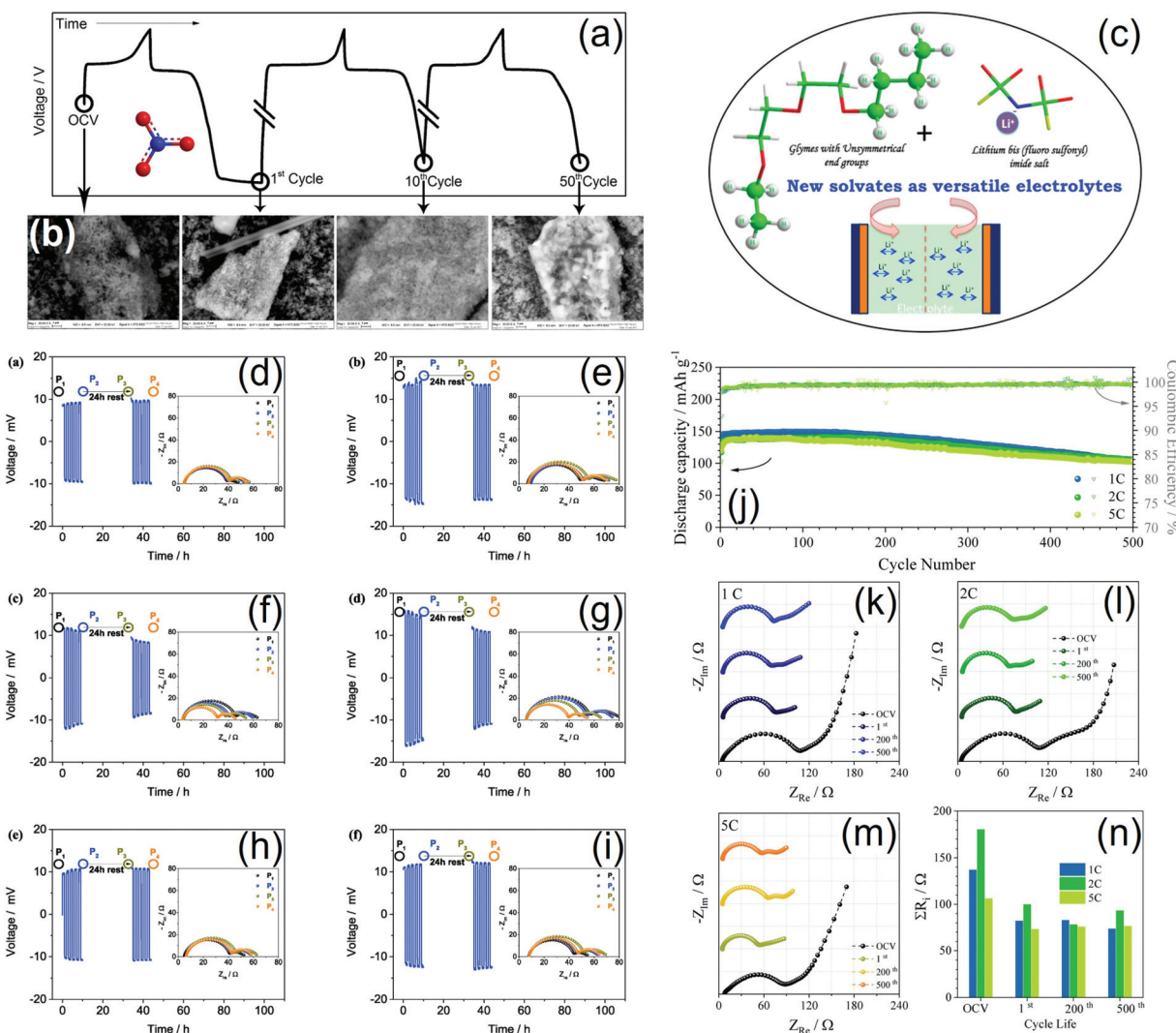


Fig. 4 (a and b) *Ex situ* SEM investigation of LiFePO_4 electrodes after cycling in a $\text{Li}|\text{G}_3\text{-LiTf-LiNO}_3\text{-LiFePO}_4$ cell under the OCV conditions (just after cell assembly and stabilization) and after the 1st, 10th, and 50th cycles; (a) voltage profiles and (b) SEM images. First discharge performed by decreasing the voltage below 2 V at a C/5 rate and limiting the time to 5.15 h; subsequent cycles within the 2–4 V voltage range at a C/5 rate (1C = 170 mA g⁻¹ with reference to the cathode mass). Reproduced with permission.⁵⁵ Copyright © 2017 American Chemical Society. (c) Schematic exemplifying the promising properties of solvates based on glymes with unsymmetrical (ethyl and butyl) end groups as electrolytes for lithium batteries characterized by high conductivity. Reproduced with permission.⁵⁶ Copyright © 2017 American Chemical Society. (d–i) Voltage profiles of lithium stripping/deposition galvanostatic cycling tests of symmetrical $\text{Li}|\text{Li}$ cells and corresponding Nyquist plots of the EIS before the test (P1), after 5 cycles (P2), upon 24 h of rest after cycling (P3), and after additional 5 cycles (P4) for (d) $\text{G}_2\text{-LiTFSI}$, (e) $\text{G}_3\text{-LiTFSI}$, (f) $\text{G}_2\text{-LiFSI}$, (g) $\text{G}_3\text{-LiFSI}$, (h) $\text{G}_2\text{-LiBETI}$, and (i) $\text{G}_3\text{-LiBETI}$. Cycling test at a constant current density of 0.1 mA cm⁻². Step time: 1 h; EIS carried out by applying an AC signal with an amplitude of 10 mV in the frequency range from 500 kHz to 100 mHz; temperature: 25 °C. Reproduced with permission.⁵⁷ Copyright © 2019 Elsevier Ltd. All rights reserved. (j) Galvanostatic cycling trend in terms of discharge capacity and coulombic efficiency over 500 cycles of a $\text{Li}|\text{LiFePO}_4$ cell using the $\text{LiTFSI-LiNO}_3\text{-G}_3$ electrolyte at 1C, 2C and 5C rates (1C = 170 mA g⁻¹ with reference to the cathode mass). (k–m) Nyquist plots of EIS measurements performed on the same cell during the cycling tests at (k) 1C, (l) 2C, and (m) 5C rates; impedance spectra were recorded under the OCV conditions, after the 1st, 200th, and 500th cycles. (n) Electrode/electrolyte interphase resistance for the same cell as extracted from the EIS data of panels k–m. Reproduced with permission.⁵⁹ Copyright © 2020 Wiley-VCH Verlag GmbH & Co. KGaA, Weinheim.

those based on Li-intercalation (LiCoO_2 and graphite layered materials) and Li-insertion (LiFePO_4 olivine and $\text{Li}_2\text{Ti}_5\text{O}_12$ spinel). Possible formation of SILs due to salt concentration changes is suggested to remarkably improve the oxidative stability of glyme electrolytes up to 5 V vs. Li/Li^+ , and the migration of G-S complexes in specific formulations is indicated to improve cell performances, depending on the current

value which is the limiting factor due to the depletion of the lithium salt in the electrode proximity. New electrodes such as $\text{LiNi}_{1/3}\text{Mn}_{1/3}\text{Co}_{1/3}\text{O}_2$ and $\text{LiMn}_{0.5}\text{Fe}_{0.5}\text{PO}_4$ can also be employed in lithium cells using a glyme-based electrolyte with a stability and efficiency depending on the upper voltage cutoff. All the measurements indicate that the control of the salt concentration at the electrode/electrolyte interphase during cell oper-

ation and the formation of a favorable SEI are the key factors for achieving the optimal operation of the lithium cells using insertion or intercalation electrodes. In particular, the addition of LiNO_3 to the electrolyte formulation as a sacrificial film-forming agent appears to significantly improve the SEI at the electrodes, in particular using glymes having longer chains such as PEGDME and adopting suitable electrochemical activation steps. We remark again that the glyme electrolyte ionic transport, electrochemical stability and interphase characteristics are substantially governed both by the salt nature and solvent chain length, and by the specific combination and experimental setup used for allowing efficient cell operation. Therefore, targeted studies are suggested for investigating the various systems and further evaluating the actual battery applicability.

4. Lithium salts in glymes: ionic liquids or concentrated solutions?

Electrolytes formed by dissolving various lithium salts in glymes differing by the ether chain length were initially considered as simple solutions, mainly characterized by the solute concentration.^{16–24} Subsequently, the concept of liquid solvated salt-complexes with similar characteristics to those of ionic liquids, *i.e.*, molten salts, was proposed.¹³³ In this regard, Raman spectroscopy may shed light on the various solvate structures occurring in the liquid phase at room temperature, whilst PFG-NMR may reveal information on the ion transport properties that can be crucial to understanding the ion–solvent interactions. Accordingly, a literature work investigated solutions of LiFSI in G_3 or G_4 , where the G_n :salt molar ratio was 1 : 1, which were identified as SILs comprising a cationic $[\text{Li}(\text{G}_n)]^+$ complex and the FSI^- anion based on Raman data. For G_n :LiFSI ratios higher than 1, anionic Li_xFSI_y complexes were formed in addition to the cationic ones. Moreover, PFG-NMR revealed that the self-diffusion coefficients of Li^+ (D_{Li}) and glyme (D_{glyme}) were the same when G_n :LiFSI was 1 : 1, which indicated that Li^+ and glyme diffuse together as a cationic $[\text{Li}(\text{G}_n)]^+$ complex. The ratio of the self-diffusion coefficients of anions and cations, $D_{\text{FSI}}/D_{\text{Li}}$, was constant at *ca.* 1.1–1.3 when G_n :LiFSI was 1 : 1 and increased as the amount of LiFSI in the solution was raised, suggesting a change in the ion transport mechanism. Furthermore, the increase in LiFSI concentration enhanced the oxidative stability of the electrolyte and mitigated the Al corrosion.⁶¹ The local structure of Li^+ ions in equimolar mixtures of glymes (G_3 , G_4) was investigated in solutions of LiTFSI, LiBETI, LiTf, LiBF₄, LiClO₄, LiNO₃, and LiTFA. Raman spectra and *ab initio* molecular orbital calculations revealed a crown-ether like conformation of the glyme molecules to form a monomeric $[\text{Li}(\text{G}_n)]^+$ complex in the molten state. Raman spectroscopic data identified the fraction of the free glyme in the $[\text{Li}(\text{G}_n)]\text{X}$ solutions (where X is the anion; see Fig. 5a), which was estimated to be a small percent in $[\text{Li}(\text{G}_n)]\text{X}$ with perfluorosulfonylimide type anions. Equimolar mixtures characterized by a low concentration of

free glyme were regarded as SILs, while those containing a substantial amount of free glyme were classified as concentrated solutions. It is worth mentioning that the concentration of free glyme decreases as the concentration of salt increases, leading to a notable increase in the lithium–metal electrode potential. The significantly high electrode potential in SILs suggested the presence of stable $[\text{Li}(\text{G}_n)]^+$ complexes in the molten state.⁶² In another work, the $[\text{Li}(\text{G}_4)]_1\text{[TFSI]}$ SIL was mixed with various polymers, *i.e.*, PEO, PMMA, and PBA, to prepare quasi-solid electrolytes for lithium batteries. The stability of the $[\text{Li}(\text{G}_4)]^+$ complex in the various solutions was assessed by comparing the ratio of the self-diffusion coefficient of glyme and Li^+ ions ($D_{\text{G}}/D_{\text{Li}}$). Thus, the $[\text{Li}(\text{G}_n)]_1\text{[TFSI]}$ solution and the composites based on PMMA and PBA behaved as ILs since $D_{\text{G}}/D_{\text{Li}} = 1$ (Li^+ and G_n diffuse together), whilst the PEO-based electrolyte was characterized by $D_{\text{G}}/D_{\text{Li}} > 1$, indicating the existence of free G_4 molecules (ligand exchange between G_4 and PEO). The highly stable $[\text{Li}(\text{G}_4)]^+$ complex (PMMA- and PBA-based solutions) led to high thermal stability, high Li^+ transference number, and a wide electrochemical stability window. Among the investigated composites, the PBA-based solutions showed the lowest glass transition temperature, little affinity towards Li^+ ions, and favorable lithium transport properties.⁶³ SAXS, Raman spectroscopy, and computational modeling provided further insight into the structure of $\text{G}_4\text{-LiTFSI}$ SILs. Indeed, a peak at $Q = 0.95 \text{ \AA}^{-1}$ in the SAXS spectra indicated structural correlations of typical ILs. This peak grew in intensity as the concentration of salt increased, reaching a maximum at the equimolar ratio (G_4 :LiTFSI 1 : 1; see Fig. 5b) due to the effective solvation of each Li^+ ion by one G_4 molecule forming a $[\text{Li}(\text{G}_4)]^+$ complex. These data were confirmed by Raman spectroscopy analyses, which suggested the occurrence of SSIPs in the solution. However, it is worth considering that even at the equimolar concentration not all Li^+ ions were solvated and minor interactions between cations and anions were observed.⁶⁴ A further report suggested that changing the G_3 :LiTFSI ratio may significantly affect the electrode/electrolyte interphase and, therefore, the cycle life of the cell. Indeed, SILs containing excess LiTFSI ensured notable mitigation of detrimental reactions between the LiCoO_2 cathode and electrolyte.⁶⁵

Glyme-based SILs typically exhibit a high viscosity, which may adversely impact the ion mobility, so various solvent additives able to enhance the conductivity of the solution have been studied. Among the diluents proposed so far, HFE demonstrated suitable properties for use in batteries. Hence, the liquid structure of HFE diluted $[\text{Li}(\text{G}_4)]_1\text{[TFSI]}$ was investigated combining Raman spectroscopy and DFT data, which suggested that the additive does not directly coordinate the Li^+ ion. SSIPs along with monodentate and bidentate CIPs were found in the neat and HFE diluted $[\text{Li}(\text{G}_4)]_1\text{[TFSI]}$, and the monodentate CIP decreased whilst the SSIP increased when diluting with HFE. HEXTS experiments were performed and supported by data of MD simulations, where the intermolecular force-field parameters, mainly partial atomic charges, were newly proposed for the HFE and glymes. A new



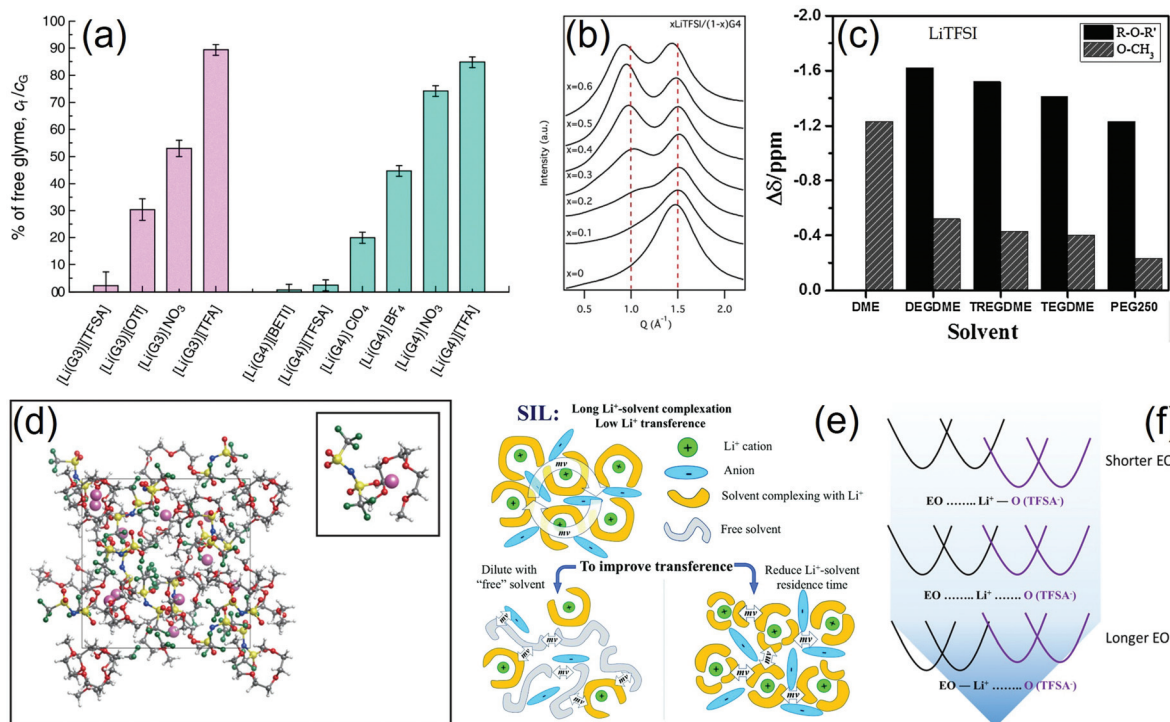


Fig. 5 (a) Estimated percentages of free glyme (c_f/c_G , where c_f and c_G are the concentration of free glyme and the total concentration of glyme in the mixture, respectively) in equimolar molten mixtures $[\text{Li}(\text{glyme})_1]\text{X}$ at 30 °C (X is TFSI, Tf, NO₃, TFA, BETI, ClO₄, and BF₄). Reproduced with permission.⁶² This journal is © the Owner Societies 2015. (b) SAXS diffraction patterns of different mole fractions of LiTFSI dissolved in G₄. The dotted vertical lines represent guidelines to the eye. Reproduced with permission.⁶⁴ Copyright © 2015 Elsevier B.V. All rights reserved. (c) Chemical shift difference of ¹⁷O resonance of glyme between Li salt solution and pure solvent ($\Delta\delta = \delta_{\text{electrolyte}} - \delta_{\text{solvent}}$) as determined by NMR experiments. Adapted with permission.⁶⁸ Copyright © 2016 Elsevier Ltd. All rights reserved. (d) Snapshot of the structure for the LiTFSI-G₃ electrolyte solution; CIP in which a Li ion is solvated by one G₃ molecule and one TFSI anion; the inset shows the representative solvation structures of the Li ion. Adapted with permission.⁶⁹ Copyright © 2016 American Chemical Society. (e) Schematic illustration of an SIL with a low Li⁺ transference number due to momentum conservation constraint and two possible strategies to facilitate the momentum exchange in the electrolyte and to increase Li⁺ transference. Reproduced with permission.⁷³ This journal is © the Owner Societies 2018. (f) Schematic illustration of the potentials of mean force (PMF = $-RT\ln g(r)$, where $g(r)$ is the pair correlation function for the Li-O atom pair) in glyme-G_n solutions, suggesting the predominance of the CIP formation for short glyme chains ($n < 4$) and preference in the Li⁺-solvate complexes for long glyme chains ($n > 4$). Reproduced with permission.⁷⁸ Copyright © 2019 American Chemical Society.

peak ascribed to the correlation between the $[\text{Li}(\text{G}_4)][\text{TFSI}]$ ion pairs was found at *ca.* 0.6–0.7 Å⁻¹ in the X-ray structure factors, and it was suggested that the terminal oxygen atoms of G₄ in the $[\text{Li}(\text{G}_4)]^+$ complex frequently repeat coordinating/uncoordinating, although almost all of the G₄ molecules coordinate the Li⁺ ions.⁶⁶ The effects of dilution with various solvents on the viscosity and the ionic conductivity of $[\text{Li}(\text{G}_n)]_1[\text{TFSI}]$ molten complexes were further studied. Nonpolar solvents, such as toluene, DEC, and HFE, formed stable $[\text{Li}(\text{G}_3)]^+$ and $[\text{Li}(\text{G}_4)]^+$ solvates, whilst ligand exchange indicating competitive solvation took place between glyme and polar solvents, such as water and PC. On the other hand, ACN exhibited intermediate properties, as it participated in the lithium solvation to form mixed $[\text{Li}(\text{G}_3)(\text{ACN})]^+$ and $[\text{Li}(\text{G}_4)(\text{ACN})]^+$ complexes. Furthermore, $[\text{Li}(\text{G}_4)][\text{TFSI}]$ was found to be more conductive than $[\text{Li}(\text{G}_3)][\text{TFSI}]$ when diluted with nonpolar solvents due to higher ionic dissociativity.⁶⁷

Natural abundance ¹⁷O NMR spectroscopy provided information on the solvation behavior of LiTf and LiTFSI in glymes

with different chain lengths, that is, G_n with $n = 1, 2, 3$, and 4 and PEGDME with MW of 250 and 500 g mol⁻¹. The chemical shifts of the glyme oxygen in the solutions and in the neat solvents were compared, revealing a more pronounced effect of the salt addition on the chemical shift of ether oxygens compared to that of terminal oxygens, which suggested a preferential coordination of Li⁺ with the ether oxygen. The NMR data showed a mitigation of the chemical-shift changes as the glyme chain length increased (see Fig. 5c), which was attributed to the increased number of ether oxygens coordinating each Li⁺. Moreover, the chemical shift of anion oxygen suggested that the long chains may decrease the ion association.⁶⁸ The solvation structure of lithium ions in the G₃-LiTFSI was determined by performing MO and MD simulations based on DFT. According to these analyses, the Li⁺ ions in the equimolar mixture were solvated mainly by crown-ether-like curled G₃ molecules and in direct contact with a TFSI⁻ anion (see the snapshot in Fig. 5d). The aggregate formed with Li⁺ and TFSI⁻ anions and/or G₃ chains was equally stable,



thereby suggesting that a small fraction of cations may form aggregates.⁶⁹ Several characteristics of the anion, such as its flexibility and its ligand properties, influence the solvate structure, as demonstrated in a computational investigation of glyme-based solutions of LiTFSI and LiTDI. The related results revealed that TFSI^- anions favor the formation of SILs, whilst TDI^- anions preferably give rise to ionic aggregates. In particular, the latter anions ensured the presence of "free" cationic species even at extremely high salt concentration.⁷⁰ Important parameters may be extracted from PGSE-NMR measurements to provide a large dataset describing various electrolyte solutions. For example, a comparative analysis of several systems formed by dissolving LiPF_6 , LiBF_4 , LiTFSI , LiBETI , LiBOB , LiTf or Li_2DFB in PC, EC, GBL, DEC, G_n (where $n = 2, 3, 4$, and 5), or PEGDME of average MW of 400 and 1000 g mol⁻¹ was carried out by plotting the Li^+ and anion diffusion constants (D_{Li} and D_{anion}) *versus* the ionic conductivity (σ). The Nernst-Einstein (NE) relationship was employed to calculate the degree of apparent ion dissociation (α) from the D_{Li} , D_{anion} and σ parameters. Furthermore, the apparent lithium transference number (t_{Li}) was determined from D_{Li} and D_{anion} , and the number of charge-carrying ions (N_{carrier}) was estimated from α and the salt concentration. Additional relationships were considered, such as σ *vs.* α , σ *vs.* N_{carrier} , and σ *vs.* t_{Li} .⁷¹ The Li^+ transport in glyme-based electrolytes was also investigated by comparing the characteristic features of various solutions, that is, 1.0 M LiTf, LiTFSI, or LiFSI in G_4 as well as 0.5, 2.0, or 2.7 M LiTFSI in G_4 . Ionic conductivity (σ), viscosity (η), and density were measured, and the self-diffusion coefficients (D) of Li^+ , anions, and solvent were determined *via* PGSE-NMR. This study suggested that the mobility (μ) in the solution is controlled by the salt, as the Lewis basicity and hardness of anions affect the Li^+ -anion and Li^+ - G_4 interactions, as well as η and D . The interaction energies (ΔE) determined by DFT calculations based on the supermolecule method were found to be in the order LiTf > LiTFSI > LiFSI, which is consistent with the dissociation degree of these salts in solutions. The study demonstrated that increasing μ and the number of carrier ions (n) is an effective way to enhance σ for glyme-based electrolytes with low dielectric constants. In this regard, suitable properties may be achieved using DME.⁷² VLF-EIS analyses of Li|Li symmetrical cells and MD simulations using atomistic, polarizable force field provided additional insight into the Li^+ transport of equimolar SILs, enabling the calculation of the three Onsager coefficients. Accordingly, a recent study of a G_4 -LiTFSI mixture (1:1 ratio) showed that even though the ionic conductivity and the Li^+ transport number (*i.e.*, the transport parameter extracted from PFG-NMR data) were acceptably high, the Li^+ transference number under anion-blocking conditions was extremely low. This observation was related to the strong complexation of Li^+ by glyme molecules, which leads to a long residence time of the solvent near the cation and causes significant anti-correlation of cation and anion motion due to the constraint of momentum conservation (see Fig. 5e). Moreover, it is worth mentioning that any transport number determined by PFG-NMR would substantially differ from the

relevant electrochemical transference number in the presence of significant ion pairing. We also remark that strongly anti-correlated motion of the cation and anion is typical of ionic liquids and, according to the structural model described above, glyme molecules complexed with Li^+ cannot ensure momentum exchange between ions. Therefore, reducing the residence time between Li^+ and solvent molecules or diluting the solution (adding excess solvent) may increase the Li^+ transference number, as depicted in Fig. 5e.⁷³ On the other hand, an unusual LiTFSP salt in a salt-in-glyme-based (salt-in-solvent) electrolyte solution exhibited predominant Li^+ conductivity with very high lithium transference numbers (70% from the polarization experiments), as well as an ionic conductivity that was three times higher than that of a solution of LiTf in G_2 . This salt-in-solvent electrolyte was studied by PFG-NMR and EIS in symmetrical Li|Li cells, which suggested a suitable lithium-conduction behavior for applications in a battery, as ascribed to the reduced mobility of large, solvated anions along with improved ionic dissociation.⁷⁴

Recently, FPMD simulations identified the solvate structure in G_4 -LiTFSI electrolyte solutions. If the salt and solvent were in an equimolar ratio, the simulations showed a positive correlation between the total coordination number of Li^+ ions and the phase stability. At the ground state of the equimolar G_4 -LiTFSI mixture, curled G_4 molecules and TFSI^- anions coordinated most of the Li^+ ions through 4 and 1 O atoms, respectively, and $[\text{Li}(\text{G}_4)_1][\text{TFSI}]$ was the second most stable CIP in gas-phase cluster calculations. If the concentration of LiTFSI was low, Li^+ ions were not in direct contact with TFSI^- anions and coordinated by two G_4 molecules. As expected, pairing between $\text{Li}(\text{G}_4)^+$ and TFSI^- was likely to occur at an equimolar ratio between the salt and solvent, leading to properties typical of ionic liquids.⁷⁵ Cell temperature and salt concentration were shown to have effects on the ionic conductivity and the Li^+ transference number of liquid-solid, glyme-based electrolytes containing nanoporous alumina. Adsorption of the anion on the surface of the alumina particles had a beneficial impact on the cation transference number, mostly at lower salt concentration and elevated temperature. Even though the lithium transference number was high, unfavorable mossy lithium deposits were observed.⁷⁶ In this regard, the performance of the lithium anode was investigated also by comparing the effect of the concentration, ether chain length, molecular structure, and electrolyte formulation of various solutions, namely, G_n -EC-LiFSI (where $n = 1, 2, 3$, and 4), DOL-EC-LiFSI and DEC-EC-LiPF₆. Conventional carbonate-based electrolytes using LiPF₆ gave rise to needle-like lithium dendrites, whereas high-concentration ether-based solutions favored knot-like and rounded lithium structures. Enhanced Li^+ -solvent interactions and fewer free molecules were found in high-concentration EC-based electrolytes. These latter solutions showed fewer side reactions with the lithium-metal anode along with significant mitigation of the dendrite formation.⁷⁷ A recent study suggested a dynamic chelating effect, which was found to be related to solvent exchange and/or contact ion-pair formation/dissociation, having significant effects on Li^+ trans-



port. Data on the pair correlation functions for the Li–O(G_n) and Li–O(TFSI[−]) pairs enabled to propose the PMF trend depicted in the schematic in Fig. 5f, which suggested the predominance of CIP and Li⁺–glyme complex formation for short-chain and long-chain solvents, respectively. According to this work, G₄ had intermediate characteristics, showing solvent exchange and CIP association/dissociation at a similar rate, which ensured high conductivity and low viscosity.⁷⁸ In agreement with these observations, a comparison of NMR diffusion and EIS data on glyme-based solutions of LiPF₆ revealed stronger ion pairing with decreasing glyme chain length. Furthermore, a decrease in the dielectric constant of the solvent with increasing temperature was suggested to further increase the ion association, thereby adversely affecting the ionic conductivity.¹³⁴

As mentioned above, the lithium transference number in glyme–salt mixtures is influenced by ion–ion anticorrelations. This aspect was further demonstrated by eNMR measurements, which revealed the migration of the species forming G₄–LiTFSI or G₄–LiBF₄ electrolytes in an electric field. Relevant data on the electrophoretic mobility and the self-diffusion coefficients for the ¹H, ⁷Li, and ¹⁹F nuclei provided insight into transference numbers, effective charges, and ionicities in various solutions characterized by a different salt concentration. In agreement with other reports, eNMR suggested that the G₄ molecule migrates along with the cation due to the formation of a stable solvate complex. Furthermore, NMR showed an increase in effective charges as the solution approached the equimolar ratio between glyme and salt and a notable difference in effective charge for lithium and anions, as well as between the G₄–LiTFSI and G₄–LiBF₄ systems. A schematic representation of the ion–ion and ion–solvent interactions in these solutions as a function of concentration and salt composition is reported in Fig. 6a. Anticorrelations between solvate cations and the anionic complexes due to momentum conservation were identified as a crucial phenomenon possibly affecting the behavior of these mixtures to a different extent, depending on the employed electrolyte formulation. In this regard, high salt concentration along with the use of smaller anions that may form large asymmetric clusters may lead to strong anticorrelation.⁷⁹ Therefore, a clear understanding of the solvate structure may elucidate the Li⁺ transport mechanisms in highly concentrated solutions, thereby providing crucial insight for electrolyte design. Concerning this point, a study of speciation in concentrated G_n–LiX and aqueous electrolyte systems identified the solvent activity and the activity coefficient in the gas phase at equilibrium with the solution as suitable parameters to classify the mixtures as SILs or superconcentrated solutions. Thus, analyses performed with a Raman/IR spectral analysis technique, which may reveal the free-solvent concentration, showed that the solution can be regarded as an SIL when the activity coefficient (*f*) is lower than 0.01. Accordingly, electrolyte solutions with the compositions of (H₂O)_{1−*x*}–LiTFSI_{*x*}, (G₃)_{1−*x*}–LiTFSI_{*x*}, and G₃–LiX (where X is NO₃[−], TFA[−], or TFSI[−]) can be classified as shown in Fig. 6b, by reporting *f* as a function of *x*, that is, the salt

molar fraction.⁸⁰ As mentioned, the Li⁺ transference number estimated using the potentiostatic polarisation method of typical SILs, such as the G₄–LiTFSI equimolar mixture, is considerably lower than the corresponding transport number estimated via PFG-NMR measurements of the self-diffusion coefficient. This experimental evidence was interpreted by considering the dynamic ion correlations (*i.e.*, cation–cation, anion–anion, and cation–anion cross-correlations) in the Onsager transport formalism, which describes the ionic conductivity σ_{ion} as given by eqn (1):

$$\sigma_{\text{ion}} = \sigma_{++} + \sigma_{--} - 2\sigma_{+-} \quad (1)$$

where σ_{++} and σ_{--} are the transport coefficients of the cation and anion, and the coefficient σ_{+-} takes into account the cation–anion correlations. The former transport coefficients can be represented, in turn, by self-terms obtained from the self-diffusion coefficients of cations (D_{Li}) and anions (D_{anion}) applying the Nernst–Einstein equation (*i.e.*, σ_{+}^{self} and σ_{-}^{self}) and distinct terms ($\sigma_{++}^{\text{distinct}}$ and $\sigma_{--}^{\text{distinct}}$) calculated as per eqn (2):

$$\sigma_{++}^{\text{distinct}} = \sigma_{++} - \sigma_{+}^{\text{self}} \quad \text{and} \quad \sigma_{--}^{\text{distinct}} = \sigma_{--} - \sigma_{-}^{\text{self}} \quad (2)$$

thereby leading to eqn (3):

$$\sigma_{\text{ion}} = \sigma_{+}^{\text{self}} + \sigma_{++}^{\text{distinct}} + \sigma_{-}^{\text{self}} + \sigma_{--}^{\text{distinct}} - 2\sigma_{+-} \quad (3)$$

Notably, the sign of $\sigma_{++}^{\text{distinct}}$, $\sigma_{--}^{\text{distinct}}$, and $2\sigma_{+-}$ reflects the above-mentioned dynamic cross correlations. Therefore, the parameters calculated by normalizing the terms of eqn (3) to σ_{ion} describe the contribution of these dynamic correlations to the ionic conductivity, as shown in Fig. 6c for the [Li(G₄)]/[TFSI] system. In this equimolar mixture, cation–cation, anion–anion, and cation–anion migrations are anti-correlated, so that $\sigma_{++}^{\text{distinct}}$ and $\sigma_{--}^{\text{distinct}}$ negatively contribute to the ionic conductivity, whilst $2\sigma_{+-}$ positively contributes to the ionic conductivity. Hence, Fig. 6c suggests that the momentum conservation of the [Li(G₄)]⁺ complex and the TFSI[−] anion is achieved by momentum exchange of the ions, as is typical of ILs. Notably, conventional concentrated solutions would instead exhibit significant momentum exchange between the ions and solvent.⁸¹ These interactions between the various species in the solution have major effects on the relationship between the Li⁺ transference number estimated via the potentiostatic polarization method ($t_{\text{Li}}^{\text{PP}}$) and the ionic conductivity (Fig. 6d). Accordingly, high $t_{\text{Li}}^{\text{PP}}$ and low ionic conductivity were observed in electrolytes containing anions with high Lewis basicity, which showed a strongly coupled, collective migration of Li⁺ cations and anions forming clusters. An example of these solutions is the [Li(G₃)]/[TFA] system, which is in fact characterized by all positive Onsager coefficients in eqn (3), thereby leading to a $t_{\text{Li}}^{\text{PP}}$ as high as 0.90, in spite of an ionic conductivity below 0.1 mS cm^{−1}. On the other hand, the $\sigma_{++}^{\text{distinct}}/\sigma_{\text{ion}}$, $\sigma_{--}^{\text{distinct}}/\sigma_{\text{ion}}$, and $\sigma_{+-}/\sigma_{\text{ion}}$ coefficients were all negative for the [Li(G₃)]/[TFSI] system, which is reflected as a relatively high conductivity and low $t_{\text{Li}}^{\text{PP}}$ (*i.e.*, about 1.1 mS cm^{−1} and 0.028, respectively). Furthermore, the five Onsager transport coefficients for [Li(G₃)]/[TFA] were larger than those of



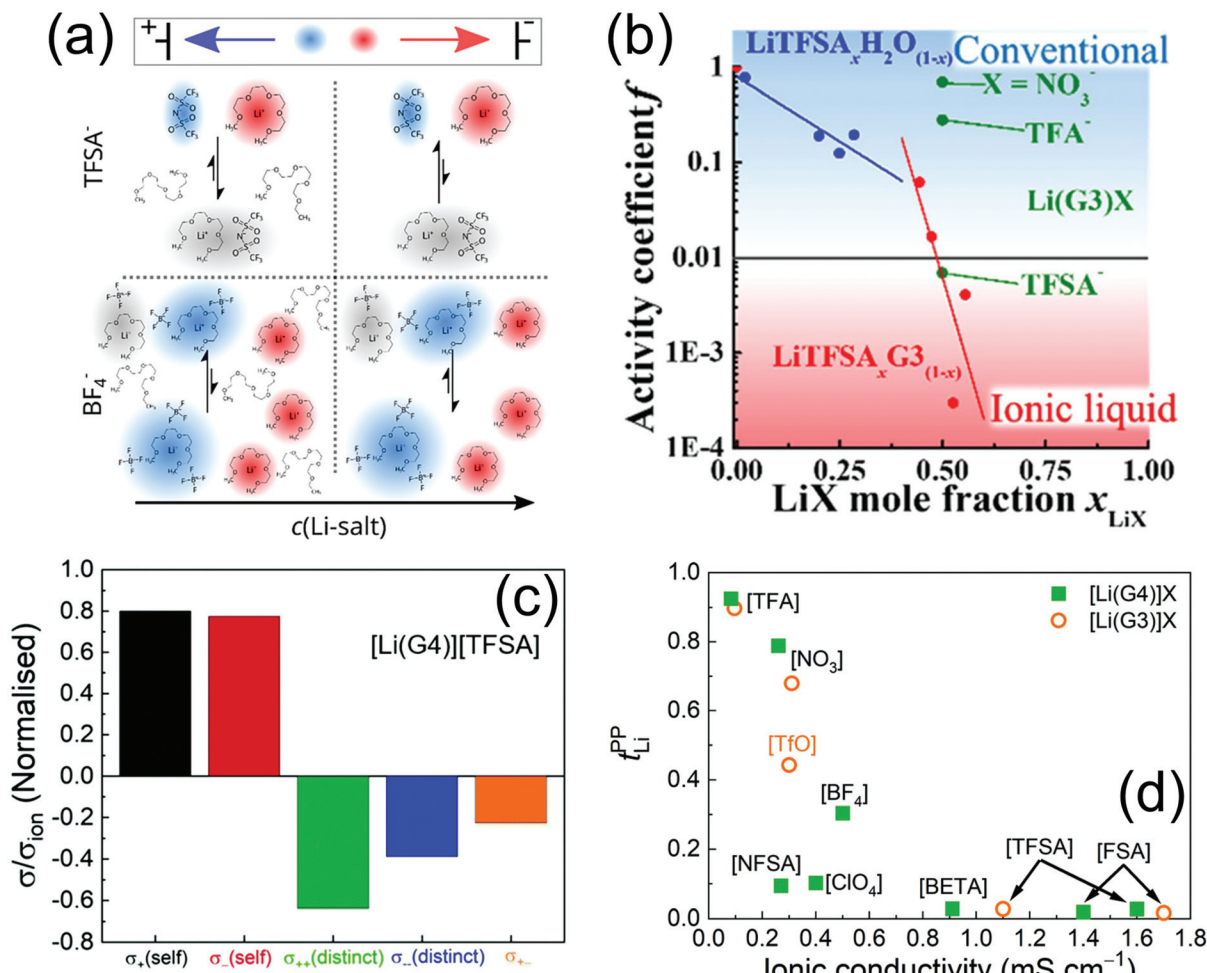


Fig. 6 (a) Schematic representation of speciation: suggested dominant ion clusters in the low and high salt concentration regimes for $[Li(G_4)_x][TFSI]$ (top) and $[Li(G_4)_x][BF_4]$ (bottom). Anionic species are depicted in blue, cationic species in red, and neutral species in gray. Reproduced with permission.⁷⁹ Copyright © 2020 American Chemical Society. (b) Plots of activity coefficients vs. Li salt mole fraction. Blue and red denote $[LiTFSI]_x(H_2O)_{1-x}$ and $[LiTFSI]_x(G_3)_{1-x}$, respectively, and green denotes $[LiX][G_3]$ ($X = NO_3^-$, TFA^- , or $TFSA^-$); $f < 0.01$ is herein used as a thermodynamic criterion for categorizing the mixture as an SIL instead of a concentrated electrolyte solution. Reproduced with permission.⁸⁰ © 2020 American Chemical Society. (c) Five transport coefficients according to the Onsager formalism ($\sigma_{+}(self)$, $\sigma_{-}(self)$, $\sigma_{+(distinct)}$, $\sigma_{-(distinct)}$, and σ_{+-} : left to right) normalized by the ionic conductivity (σ_{ion}) of the molten Li salt solvates for the $[Li(G_4)][TFSI]$ complex. Adapted with permission.⁸¹ This journal is © the Owner Societies 2020. (d) Plots of the Li^+ transference number based on potentiostatic polarization measurements (t_{Li}^{PP}) vs. ionic conductivity for $[Li(G_n)]X$ complexes ($n = 3$ and 4; $X = TFA$, NO_3 , Tf , BF_4 , $NFSA$, ClO_4 , $BETI$, $TFSI$, and FSI). Reproduced with permission.⁸² This journal is © the Owner Societies 2021.

$[Li(G_3)][TFSI]$ by about two orders of magnitudes due to the low ionic conductivity of the former electrolyte.^{81,82}

The data reported above clarify in part the features of electrolytes formed by dissolving salts in glymes. Under specific concentrations, the G-S systems were classified as liquid solvated salts (SILs), similar to ionic liquids (ILs), in which both cations and anions contribute to the ionic conductivity. The free-glyme fraction is the parameter taken into account for rationalizing the G-S characteristics. Indeed, solutions with a low free-glyme fraction belong to the SILs, particularly using G_3 and G_4 , whilst those with a high free-glyme fraction belong to the concentrated solution class. The stability of $[Li(G_n)]^+$ complexes, strongly depending on the glyme chain length and the anion nature, affects the thermal stability and Li-transfer-

ence number of the electrolyte. Furthermore, the formation of SILs can increase the electrolyte viscosity and hinder ion mobility and cell performances. The use of nonpolar additives in the glyme solutions can actually increase the ion mobility without altering the Li-solvent coordination and structure, which is instead changed by polar additives. In addition, the coordination of Li^+ ions to the ether-oxygen which plays a key role in allowing the formation of complexes is correlated with the salt concentration. For example, the formation of crown complexes and aggregates compatible with SILs is observed when salts having the $TSFI^-$ anion are used at low concentration. Interestingly, both the mobility and viscosity of the glyme electrolyte are controlled by the Lewis basicity and hardness of the anions, while the number of ion carriers and the

ionic conductivity increase using glymes with relatively low dielectric constants. Moreover, the strong interactions between glyme chains and Li^+ occurring in concentrated solutions can increase the residence time of the solvent near the ions, thus decreasing the Li^+ -transference number. Therefore, diluted solutions have typically a higher Li^+ -transference number than concentrated ones, except for some particular cases (e.g., the solvent-in-salt electrolytes in which very large anions are used to remarkably increase the t_{Li^+}). The temperature affects the formation of SILs that, in turn, govern the growth of the lithium dendrites at the metal surface. Indeed, diluted solutions may favor the formation of needle-like dendrites, and instead knot-like and rounded lithium structures can be formed in concentrated solutions. Interestingly, predominant CIP formation and stronger ion pairing are observed in electrolytes using short-chain glymes compared to those using long-chain glymes, in which Li^+ -glyme complexes are preferentially formed, whilst the ion association degree is modified by changing the temperature value which directly affects the dielectric constant. Furthermore, ion-ion anticorrelation with the migration of G-S clusters within the electric field is affected by the salt concentration and anion size, where high concentrations and small ions lead to large asymmetric clusters with strong anticorrelation. Most likely, the glyme solutions can be regarded as SILs when the activity coefficient (f) is lower than 0.01, and the increase of the anion's Lewis basicity favors the lithium transference number, however depressing the ionic conductivity. Taking into account the incomplete scenario depicted by the several findings reported above, we can reasonably suggest further more systematic studies aimed at fully rationalizing the complex features of the glyme-based electrolyte since they are actually assuming an increasing importance in view of their possible application in a new generation of energy storage systems, as will be illustrated in the subsequent paragraphs.

5. "Glyme electrolyte" in a Li–S cell: a battery close to practical applications

Glymes dissolving lithium salts appeared very promising candidates as lowly flammable electrolytes for application in efficient and high-energy Li–S batteries. These cells react *via* a multielectron conversion process delivering a theoretical specific capacity as high as 1675 mA h g⁻¹ (with reference to the mass of sulfur), which is reflected as a gravimetric energy density of *ca.* 3600 or 2600 W h kg⁻¹ with reference to the mass of sulfur or Li_2S , respectively.¹³⁵ The electrochemical conversion of sulfur and lithium occurs at about 2.4 and 2.1 V *vs.* Li^+/Li according to eqn (4):



This reaction involves lithium polysulfide intermediates (Li_2S_x with $2 \leq x \leq 8$), which dissolve in common electrolyte media for $x > 2$, giving rise to complex, potential-dependent

equilibria between various species with different oxidation states.¹³⁶ Accordingly, Li–S cells undergo a gradual cathode loss in the electrolyte solution upon the electrochemical process, which may worsen the cycling performance and typically requires the optimization of a suitable cell design differing from that of conventional lithium-ion batteries. So far, a great deal of effort has been devoted to mitigating the detrimental effects of polysulfide dissolution, which has been regarded as one of the most challenging issues presently hindering practical applications of Li–S batteries. In this regard, the electrolyte formulation can radically affect the pathways of electrochemical reaction and, thus, the cell performance.¹³⁷

A pioneering work reported the characteristic features of two lithium cells employing a pitch carbon-coated Li_2S cathode and a solid-state $\text{PEO}_{20}\text{LiTf}-\text{Li}_2\text{S}-\text{ZrO}_2$ electrolyte (LiTf/EO molar ratio of 1 : 20) or a $\text{G}_4\text{-LiTf}$ liquid electrolyte (G_4/LiTf molar ratio of 1 : 4), respectively. The former battery delivered a stable capacity of 500 mA h g _{$\text{Li}_{2\text{S}}$} ⁻¹ when cycled at a C/3 rate and at 80 °C, while the latter battery exhibited a lower capacity, which is about 300 mA h g _{$\text{Li}_{2\text{S}}$} ⁻¹, when tested at a C/6 rate and at 30 °C.⁸³ A more recent work reported a lithium-sulfur polymer battery using solid PEGDME (MW 2000 g mol⁻¹) operating at 50 °C with the capacity approaching 700 mA h g _{S} ⁻¹ over 90 charge/discharge cycles. The polymer electrolyte showed high thermal stability and a stable interphase during the Li–S conversion process at 2.2 V *vs.* Li^+/Li .¹⁰⁴ Besides, $[\text{Li}(\text{G}_3)_4][\text{TFSI}]$ and $[\text{Li}(\text{G}_3)_1][\text{TFSI}]$ complexes were investigated as electrolyte solutions possibly able to mitigate the polysulfide dissolution. Indeed, a Li–S cell using the $[\text{Li}(\text{G}_3)_1][\text{TFSI}]$ complex delivered a discharge capacity higher than 700 mA h g _{S} ⁻¹ with a coulombic efficiency above 98% over more than 400 cycles. Further evidence suggested that the addition of a nonflammable fluorinated solvent that preserves the solvate complex structure may improve the rate capability of the battery.⁸⁴ Following this trend, $\text{G}_n\text{-LiX}$ equimolar mixtures (where $n = 3$ or 4 and X is BETI^- , TFSI^- , Tf^- , BF_4^- , or NO_3^-) were investigated in Li–S cells and the dissolution of lithium polysulfides (Li_2S_x) was measured. According to this study, electrolytes exhibiting SIL characteristics such as $[\text{Li}(\text{G}_n)][\text{BETI}]$ and $[\text{Li}(\text{G}_n)][\text{TFSI}]$ may effectively ensure the mitigation of the Li_2S_x dissolution, as shown in Fig. 7a. We remark that equimolar SILs would not contain "free" solvent molecules that can solvate the Li_2S_x species, as widely discussed in the previous section. On the other hand, lithium polysulfides were highly soluble in concentrated solutions, such as $\text{G}_n\text{-LiTf}$ and $\text{G}_n\text{-LiNO}_3$ (Fig. 7a). Therefore, the batteries employing SILs ensured a stable response in galvanostatic cycling test, delivering a capacity between 600 and 700 mA h g _{S} ⁻¹ with a coulombic efficiency above 98% over 100 cycles, whereas those using concentrated solutions displayed the worst performances. Moreover, the typical irreversible reduction of NO_3^- anions at the positive electrode during discharge was observed, whilst BF_4^- anions gave rise to detrimental side reactions with the polysulfide anions leading to undesired byproducts.⁸⁵ Alongside these remarkable effects of the anions, the G_n chain length was shown to have a significant influence on the mobi-



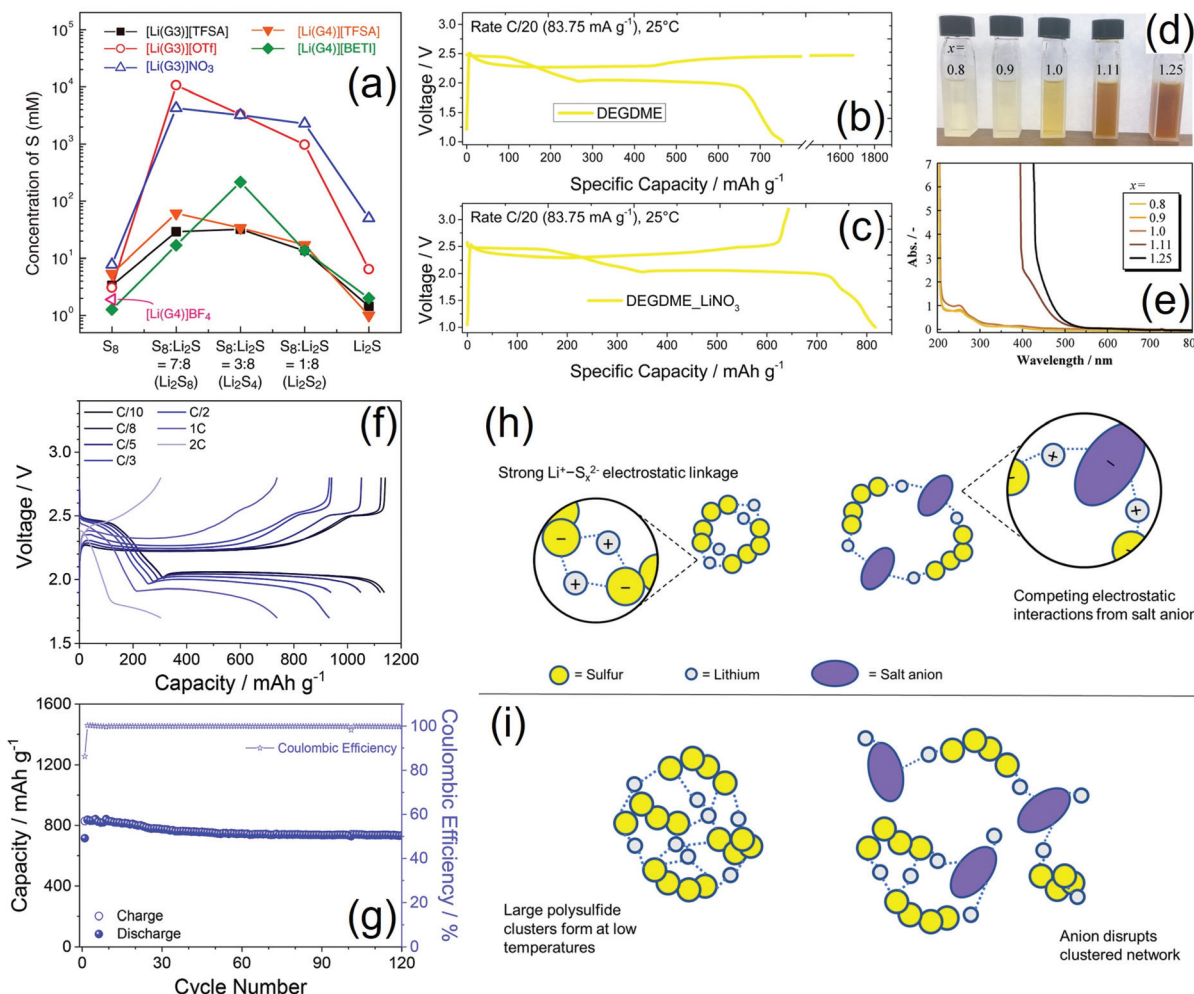


Fig. 7 (a) Solubility limits of S₈, Li₂S₈, Li₂S₄, Li₂S₂, and LiS₂, where Li₂S_m ($m = 8, 4, 2$) is the nominal formula of the mixture prepared using stoichiometric amounts of S₈ and Li₂S; the nominal formula assumes a complete reaction between S₈ and Li₂S without occurrence of disproportion reactions; [Li(glyme)]X represented by empty and full symbols are categorized as SIs and concentrated solutions, respectively. Reproduced with permission.⁸⁵ Copyright © 2013 American Chemical Society. (b and c) Voltage profiles of Li-S cells using (b) G₂-LiTf (LiTf in a concentration of 1 mol kg_{solvent}⁻¹) and (c) G₂-LiTf-LiNO₃ (LiTf and LiNO₃ in concentrations of 1 mol kg_{solvent}⁻¹ and 0.4 mol kg_{solvent}⁻¹, respectively); temperature: 25 °C; voltage range: 1.2–3.2 V; current rate: C/20 (83.75 mA g⁻¹ with reference to the cathode mass). Adapted with permission.⁸⁶ Copyright © 2015 American Chemical Society. (d) Photograph and (e) UV-vis spectra of [Li(G₃)_x][TFSI] solutions of Li₂S₈ ($x = 0.8, 0.9, 1.0, 1.11$, and 1.25) diluted four times with HFE at room temperature. Reproduced with permission.⁹⁸ Copyright © 2019 WILEY-VCH Verlag GmbH & Co. KGaA, Weinheim. (f and g) Electrochemical behavior of a catholyte-based, Li|G₂-Li₂S₈-LiNO₃-LiTf|C cell in terms of (f) voltage profiles at C/10, C/8, C/5, C/3, C/2, 1C and 2C rates (1C = 1675 mA g_s⁻¹) and (g) trend of charge and discharge capacities per positive electrode and coulombic efficiency at a C/3 rate (1C = 1675 mA g_s⁻¹) as a function of the cycle number (both LiTf and LiNO₃ in concentrations of 1 mol kg_{solvent}⁻¹); voltage range: 1.8–2.8 V from C/10 to C/3 and 1.7–2.8 V from C/2 to 2C. Adapted with permission.⁹⁹ Copyright © 2018 Elsevier B.V. All rights reserved. (h and i) Illustration of competing interactions between lithium species in electrolyte solutions for Li-S batteries; (h) strong Li⁺-S_x²⁻ bond networks disrupted from competing electrostatic interactions between lithium ions and lithium salt anions; and (i) lithium polysulfides that naturally form at low temperatures, disrupted from the influence of competing lithium salt anions. Reproduced with permission.¹⁰⁰ Copyright © 2020 American Chemical Society.

liety of the various species in the electrolyte solution, thereby remarkably impacting the Li-S cell behavior. Furthermore, the beneficial effects on the “polysulfide-shuttle” process of the addition of LiNO₃ along with LiTf to the electrolyte formulation were widely demonstrated. This adverse process consists in an apparent charging without actual energy storage due to the simultaneous oxidation of polysulfides at the cathode and their direct reduction at the anode upon migration in the solution across the cell separator. In this regard, Fig. 7(b and c)

shows that the ineffective charge of a G₂-LiTf cell employing a G₂-LiTf electrolyte (see panel b) is actually suppressed after the addition of LiNO₃ to the solution (see panel c).⁸⁶ Another work proposed that the dissociation of polysulfide dianions to radicals, and particularly the trisulfur radical (S₃^{·-}), may play a crucial role in the electrochemical behavior of the Li-S cell. Accordingly, *operando* XANES measurements revealed the presence of these radicals in batteries using solutions of LiClO₄ and LiNO₃ in either G₄ or DMA, thereby suggesting that S₃^{·-}

existed in minor concentration in glymes and in relatively high concentration in electron pair donor solvents. Notably, a high degree of dissociation of the anion precursor, S_6^{2-} , to the tri-sulfur radical in the latter solvents allowed the full utilization of both S and Li_2S . As shown in this study, catholyte-based batteries would benefit from low-volatility and electron pair donor solvents, and the combination of a highly adsorptive cathode with a highly dissociative solvent could be extremely effective in ensuring a superior performance. On the other hand, electron pair donor solvents would be detrimental to achieving polysulfide-entrapping in the cathode.⁸⁷ It is worth mentioning that the Li–S chemistry would affect also the lithium-passivation properties of the glyme based solution, as shown by a literature report which provided relevant XPS and electrochemical data on G_4 –LiTf solutions charged by various polysulfide species, that is, Li_2S_2 , Li_2S_4 , Li_2S_6 , and Li_2S_8 . The results of this work demonstrated the presence of S-containing species in the SEI layer deposited over the lithium–metal anode and showed that the presence of polysulfides in the solution decreased the resistance of this layer. The addition of Li_2S_x in the electrolyte stabilized the electrode/electrolyte interphase resistance and had a buffer effect which mitigated the cathode dissolution, leading to an improvement of the Li–S cell performance.⁸⁸

Further approaches to reduce the polysulfide shuttling involved the design of electrolyte membranes with intrinsic microporosity, which would ensure size- and ion-selective transport. Polymeric membranes were optimized *via* MD simulations of the solvate structures of LiTFSI with lithium polysulfides (Li_2S_x , where $x = 8, 6$, and 4) in glymes of different chain lengths. These simulations suggested that a pore size lower than 1.2–1.7 nm might block the polysulfide crossover, thus possibly enabling a suitable electrochemical behavior of redox-flow, lithium–sulfur batteries, even in the absence of $LiNO_3$ in the electrolyte formulation.⁸⁹ Alternative strategies recently explored to improve the cycle life and rate capability of Li–S cells included the addition of support solvents to SILs based on G_n –salt complexes. An example is represented by a novel fluorinated ether derivative, *i.e.*, TFTFE, which was added to the $[Li(G_4)_1][TFSI]$ equimolar mixture, thereby enhancing the ionic transport across the electrolyte and, thus, the rate capability of the Li–S battery. Moreover, TFTFE was shown to decrease the solubility of lithium polysulfides in the electrolyte due to its low donor ability which limits the Li^+ solvation.⁹⁰ Another study comparing several equimolar mixtures of either G_3 or G_4 with various salts ($LiBETI$, $LiBF_4$, $LiTf$ and $LiNO_3$) revealed that the dissolution of lithium polysulfides may be suppressed when SILs are employed.⁹¹ On the other hand, the G_4 –LiTf solution with the lithium salt in a 1 mol kg^{-1} concentration was considered the preferred electrolyte for performing a comparative evaluation of the electrochemical performance of several cathode composites prepared by mixing sulfur with carbon materials of various characters (namely, graphite, mesocarbon microbeads, and multi-walled carbon nanotubes). Besides, the electrolyte characteristics in terms of 1H , 7Li , and ^{19}F nucleus self-diffusion coefficients, ionic conductivity, and

ionic association degree were investigated by combining NMR and impedance spectroscopy measurements. Notably, the best composite in the Li–S cell using this electrolyte achieved a capacity higher than 500 mA h g^{-1} over 140 cycles, with no sign of dendrite formation or any shuttle reaction.⁹² Glymes were also employed in combination with micropore-rich activated carbon incorporating sulfur,^{93,96} as well as with S-Ketjenblack composites showing promising results.⁹⁴ Other cathode chemistries have been explored, such as a TiS_2 –S composite reacting *via* intercalation of Li^+ ions into TiS_2 along with Li–S conversion.⁹⁵ Furthermore, a SIL consisting of a $[Li(G_4)][TFSI]$ equimolar mixture was investigated as a possible electrolyte for lithium-ion and silicon–sulfur batteries. In detail, pre-cycling in a FEC-containing solution before the test in the glyme-based electrolyte was shown to be an effective strategy to form a stable SEI incorporating fine LiF grains and organo-fluorine compounds over a Si-flake anode, which ensured a remarkable enhancement of the capacity retention.⁹⁷

A recent work provided additional evidence of the effect of the lithium-salt concentration on the solubility of polysulfides in the electrolyte solution, which has been generally attributed to the presence of “free” glyme molecules favoring the solvation of Li_2S_x species, as indeed mentioned above. In this regard, $[Li(G_n)]X$ complexes in equimolar mixtures (where LiX is a typical salt) can be locally destroyed to form “free” glyme chains upon the electrochemical process in Li–S cells. Therefore, non-equimolar mixtures (where the $G_n:LiX$ molar ratio is higher than 1) may actually decrease the concentration of dissolved Li_2S_8 , thereby improving the reversible capacity and the cycling stability, whilst increasing the coulombic efficiency. Photographic images (Fig. 7d) and UV/vis spectra (Fig. 7e) of various Li_2S_8 -containing $[Li(G_3)_x][TFSI]$ SILs with x values of 0.8, 0.9, 1.0, 1.11, and 1.25, which were diluted with HFE, are consistent with a decrease in the solubility of Li_2S_8 at increasing concentration of LiTFSI.⁹⁸ Although the mitigation of the dissolution of lithium polysulfides in the electrolyte has been regarded as a valuable strategy to enable high-performance Li–S batteries, several works have suggested that long cycle life and high coulombic efficiency may be achieved even in catholyte-based, semi-liquid configurations, provided that the lithium–metal anode is effectively protected against parasitic reactions with dissolved Li_2S_x . Catholyte solutions of polysulfides formed by dissolving either LiTFSI or LiTf as salts along with $LiNO_3$ as an anode-protection additive in G_2 were lately employed in Li–S cells exhibiting notable performances in terms of specific capacity, capacity retention, and coulombic efficiency. These solutions had suitable characteristics for applications, that is, satisfactory Li^+ transport ability, a wide electrochemical stability window, and good Li-passivation properties. Semi-liquid cells using dissolved Li_2S_8 with overall sulfur loading ranging from 3 to 6 mg cm^{-2} displayed a high rate capability, delivered a maximum capacity of *ca.* 1100 mA h g^{-1} at a C/10 rate (Fig. 7f), and ensured a stable capacity of about 800 mA h g^{-1} at a C/3 rate with the coulombic efficiency exceeding 99% (Fig. 7g).⁹⁹ Notably, the electrostatic



attraction forces between the Li^+ cation, salt anion, and S_x^{2-} anion would play a significant role in determining the solvate structures in the electrolyte solution, thus significantly affecting the behavior of the cell. Testing under low-temperature conditions shed light on this point, revealing that lithium polysulfides may form clusters that adversely impact the Li–S conversion kinetics. Therefore, a low testing temperature may lead to poor performance, despite the low freezing point and high ionic conductivity of the glyme-based electrolyte. More abundant $\text{Li}^+ \text{--} \text{S}_x^{2-}$ bonds and polysulfide clusters are formed whenever the cation has a higher affinity towards the S_x^{2-} anion rather than the salt anion. On the other hand, it was suggested that a strongly bound lithium salt would disrupt polysulfide aggregates ensuring a substantially improved low-temperature performance. A graphical schematic of the polysulfide clustering mechanism based on competing forces in the electrolyte solution is shown in Fig. 7(h and i).¹⁰⁰ Another study of the cathode dissolution in the electrolyte during operation of the Li–S cell showed that lithium polysulfides are formed in both glyme-based and fluorinated-ether-based electrolytes, in which the polysulfides are highly soluble and lowly soluble, respectively. However, lithium polysulfides were trapped in the cathode pores when the latter solutions were employed, and the polysulfide concentration in the separator was below the limit of detection of HPLC analyses, thereby suggesting a decrease of interaction between dissolved polysulfides in fluorinated-ether-based electrolytes. The different behavior of glyme-based and fluorinated-ether-based electrolytes affected the length and potential of the voltage plateaus of the battery upon cycling.¹⁰¹ The presence of Li_2S_x in the electrolyte solution may have additional major effects on the cell response by influencing the composition of the SEI, as mentioned above and recently investigated.¹⁰²

The Li–S battery is presently considered the most energetic and promising energy storage system for future practical applications. However, this alternative battery requires suitable electrolytes for allowing an adequate electrode/electrolyte interface and, at the same time, compatibility with lithium metal and low flammability. A further characteristic required is the compatibility of the electrolytes with the polysulfides, which are unavoidably formed in the cell. Alongside PEO-based electrolytes, those using glymes, in particular with the longer chain-length, appear the most promising candidates for achieving the abovementioned targets. Hence, solutions based on G_2 , G_3 , and G_4 with the addition of LiNO_3 as the sacrificial film-forming agent to suppress the polysulfide shuttle, as well as liquid and solid PEGDME can be successfully employed as the electrolyte media for Li–S cells. Interestingly, electrolytes with SIL characteristics described above appear to limit the polysulfide dissolution due to the absence of free solvent molecules, while polysulfides are soluble in concentrated solutions. Furthermore, formation of radicals during the electrochemical process of the battery affecting the stability may be limited by using glymes with long chains. The presence of polysulfides in combination with LiNO_3 as the additive actually stabilizes the lithium metal interphase, and therefore solutions of polysulfides

are proposed as the catholyte to operate in Li–S batteries. It is worth mentioning that polymeric and porous membranes are also proposed with certain success of mitigating the polysulfide shuttle effect even in the absence of LiNO_3 ; however the use of the former is suggested alongside the improvement of the cathode material. Lithium salt concentration and its nature modify the structure of G–S and change the polysulfide clustering, thus remarkably affecting the performance of the cell. An interesting example is that of the non-equimolar G–S mixtures that decrease the solubility of the Li_2S_8 intermediate and enhance the battery stability; despite this, dissolved Li_2S_8 can be actually used as the liquid cathode in Li–S cells with LiNO_3 .

6. "Glyme electrolyte" in a $\text{Li}-\text{O}_2$ battery: the upcoming future

The $\text{Li}-\text{O}_2$ cell is an appealing next-generation battery system which may possibly ensure a notable breakthrough in energy density. This technology is based on reaction (5) of oxygen with lithium in the electrochemical cell to produce lithium peroxide, occurring at 2.96 V vs. Li^+/Li and delivering a formal specific capacity of 1168 mA h g^{-1} with reference to the mass of Li_2O_2 .



However, the development of $\text{Li}-\text{O}_2$ batteries presents several challenges to overcome, which are mostly associated with parasitic reactions upon cell operation limiting the reversibility of the electrochemical process.^{138,139} Furthermore, the carbonate-based electrolytes employed in conventional lithium-ion batteries decompose in contact with the electrochemical process intermediates, that is, superoxide radical and peroxide,^{140,141} so they cannot be used in $\text{Li}-\text{O}_2$ cells. On the other hand, excessively volatile ether solvents would pose serious limitations for a system designed for potentially operating in open air.¹⁴² In this regard, glymes are considered suitable solvents for $\text{Li}-\text{O}_2$ batteries,¹⁴³ since they show high chemical stability as well as a boiling point and volatility that can be modulated by modifying the chain length.¹⁹

The applicability of $\text{G}_4\text{--LiTf}$ in $\text{Li}-\text{O}_2$ cells was initially demonstrated by elucidating the reaction mechanism in a PEO– G_4 –LiTf plasticized system. The results suggested that the highly solvating, base-resistant PEO plasticized by the low-molecular-weight, end-capped G_4 is a very good medium to study the electrochemical processes attributed to peroxide and oxide species in water-free $\text{Li}-\text{O}_2$ cells.¹⁰⁵ Subsequently, another work demonstrated that the use of a liquid $\text{G}_4\text{--LiTf}$ electrolyte solution and an appropriate cell design can allow the $\text{Li}-\text{O}_2$ system to reversibly cycle at a current rate as high as 3 A g^{-1} delivering an outstanding capacity of 5000 mA h g^{-1} (Fig. 8a). As is widely established in the $\text{Li}-\text{O}_2$ community, these values are with reference to the mass of carbon in the electrode film, that is, $\text{A g}_{\text{carbon}}^{-1}$ and $\text{mA h g}_{\text{carbon}}^{-1}$, respectively.¹⁰⁶ The electrolyte formulation significantly affects the



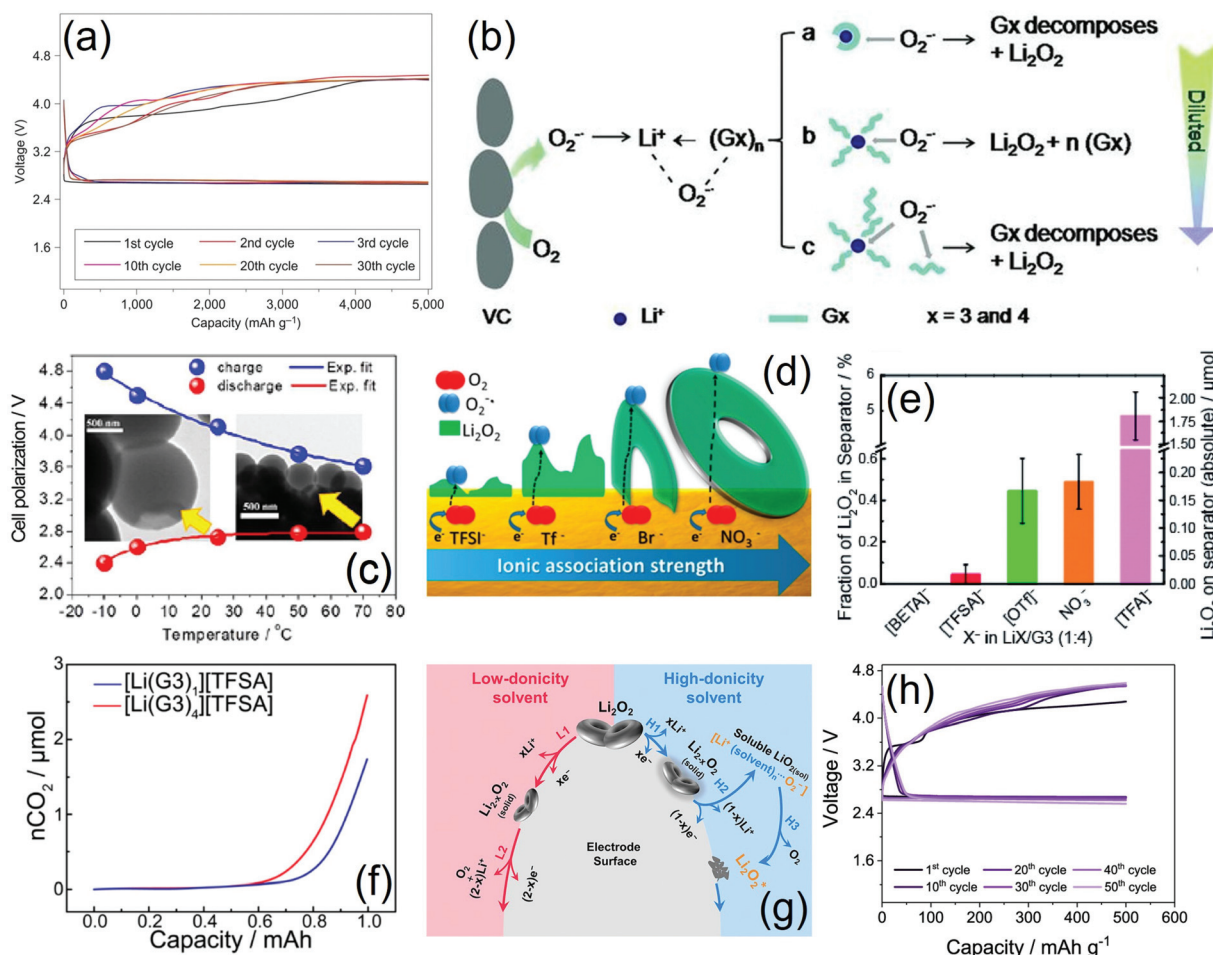


Fig. 8 (a) Voltage profiles of a Li|G₄-LiTf|O₂ battery under a 5000 mA h g⁻¹ specific-capacity limit with reference to the mass of carbon cast on the cathode GDL; current rate: 500 mA g⁻¹ (current rate with reference to the mass of carbon cast on the cathode GDL). Adapted with permission.¹⁴⁴ Copyright © 2012 Macmillan Publishers Limited. All rights reserved. (b) Mechanism of the O₂ reduction reaction in a Li-O₂ cell at the interface between carbon black and glyme-LiTFSI electrolyte solution during discharge as proposed elsewhere. Reproduced with permission.¹⁰⁹ Copyright © 2013 WILEY-VCH Verlag GmbH & Co. KGaA, Weinheim. (c) Trends of charge (blue) and discharge (red) voltage vs. temperature for a Li-O₂ cell using a G₄-LiTf electrolyte solution. Insets: *ex situ* TEM images of the cathode of the same cell after galvanostatic discharge at 25 °C (left-hand side) and at 70 °C (right-hand side); capacity limited to 10 000 mA h g⁻¹ with reference to the mass of carbon cast on the cathode GDL; current rate: 500 mA g⁻¹ (current rate with reference to the mass of carbon cast on the cathode GDL). Reproduced with permission.¹¹¹ Copyright © 2013 American Chemical Society. (d) Schematic representation of the effect of salt anions (i.e., TFSI⁻, Tf⁻, Br⁻, and NO₃⁻) in electrolyte solutions based on G₂ on the kinetics and thermodynamics of the ORR, as well as on the morphology of electrodeposited Li₂O₂ in Li-O₂ batteries. Reproduced with permission.¹¹⁷ Copyright © 2016 American Chemical Society. (e) Results of quantitative determination of Li₂O₂ on the separator in a Li-O₂ cell using LiX/G₃ (1:4) electrolytes, where X⁻ = BETI⁻, TFSI⁻, Tf⁻, NO₃⁻, and TFA⁻. The values on the left y-axis are the percentage of the amount detected in the separator with respect to the amount of total expected (theoretical) Li₂O₂ present in the cell after discharge to 1 mA h cm⁻², whilst the corresponding absolute values (μmol) are shown on the right y-axis; error bars denote the standard error. Adapted with permission.¹¹⁹ Copyright © 2017 The Chemical Society of Japan. (f) Integrated CO₂ evolution during charge of Li-O₂ cells using either [Li(G₃)₁][TFSI] (blue curve) or [Li(G₃)₄][TFSI] (red curve) electrolytes, which was calculated from electrochemical MS data, after galvanostatic discharge to 1 mA h. Adapted with permission (<https://pubs.acs.org/doi/10.1021/acsami.6b14449>).¹²² Copyright © 2017 American Chemical Society. Further permission related to the material excerpted should be directed to the American Chemical Society. (g) Solvent-controlled Li₂O₂ decomposition mechanism in Li-O₂ batteries as proposed elsewhere; "H" denotes high-donicity solvent and "L" denotes low-donicity solvent. Li₂O₂* denotes the Li₂O₂ generated by LiO₂(sol) disproportionation, where LiO₂(sol) is a soluble discharge intermediate product of the ORR. Reproduced with permission.¹²⁵ Copyright © 2018 Elsevier Inc. (h) Voltage profiles of a Li-O₂ cell using G₃-LiTFSI-LiNO₃ (both LiTFSI and LiNO₃ at concentrations of 2 mol kg_{solvent}⁻¹); specific capacity limited to 500 mA h g⁻¹ with reference to the mass of carbon cast on the cathode GDL; current rate: 100 mA g⁻¹ (current rate with reference to the mass of carbon cast on the cathode GDL); carbon loading over the cathode GDL: 0.65 mg cm⁻² (carbon mass: 1.3 mg, geometric electrode area: 2 cm²) voltage range: 1.5–4.6 V; cell aged for 7 days before cycling. Adapted with permission.¹³⁰ Copyright © 2020 American Chemical Society.

electrochemical performance and the discharge products of Li-O₂ cells. Indeed, in a further study the use of glymes as solvents led to a large amount of Li₂O₂ in the positive electrodes

after discharge, while only a small amount of Li₂O₂ was detected after discharge in electrolytes based on nitrile, ionic liquids, phosphate, and sulfoxide. The employed solvent also



influences the relative amount of Li_2CO_3 and LiF , which are formed as byproducts *via* oxidation and decomposition of the solvent and *via* the attack of superoxide radical anions on the binder and/or the F-containing imide salt, respectively. This work suggested the dibutyl diglyme as the most suitable solvent among those taken into account.¹⁰⁷ Therefore, glyme-based solutions have been so far extensively investigated as electrolytes for $\text{Li}-\text{O}_2$ cells with promising results, and alternative chemistries have also been suggested. Accordingly, there is a pioneering report on the behavior of a lithium-ion-air battery where the metal anode is replaced by a lithiated silicon-carbon composite effectively employing a $\text{LiTf}-\text{G}_4$ electrolyte solution.¹⁰⁸ Besides the salt and solvent nature, the salt/solvent molar ratio plays a crucial role in the oxygen-conversion mechanism in the cell, as demonstrated by comparing a series of solutions of LiTFSI in G_3 and G_4 with various concentrations. According to this study, the $\text{O}_2^{\cdot-}$ radical and solvated Li^+ would form an intermediate complex at the electrode/electrolyte interphase, that is, $\text{Li}^+(\text{G}_x)_n\cdots\text{O}_2^{\cdot-}$ (Fig. 8b), leading to the formation of CIP solvates containing one Li^+ ion which is coordinated with four or five oxygen atoms of one glyme molecule in concentrated solutions (route a). A decomposition pathway *via* reaction of $\text{O}_2^{\cdot-}$ with the glyme was therefore proposed (route a in Fig. 8b) to elucidate the performance degradations of $\text{Li}-\text{O}_2$ cells employing concentrated solutions. Dilution would gradually produce a mixture of (i) CIP and SSIP solvates, (ii) SSIP solvates (route b in Fig. 8b), and eventually a mixture of SSIP solvates and free glyme molecules (route c in Fig. 8b). Thus, intermediate concentrations would favor the accessibility of $\text{O}_2^{\cdot-}$ to Li^+ and decrease the interactions between $\text{O}_2^{\cdot-}$ and the glyme molecule that lead to detrimental decompositions (route b), whilst low concentrations would reasonably increase the frequency of collision between $\text{O}_2^{\cdot-}$ and glyme, thereby enhancing the parasitic processes (route c). Therefore, the glyme/salt molar ratio of 5 to 1 was found to be critical for the cycling performance of the cell, and high stability over 20 cycles at 500 mA $\text{g}_{\text{carbon}}^{-1}$ was demonstrated using $(\text{G}_n)_5\text{-LiTFSI}$ electrolytes with $n = 3$ and 4.¹⁰⁹ The electrolyte purity is another crucial aspect that should be taken into account, as shown in a qualitative and quantitative investigation of the reaction of KO_2 with glymes of various chain lengths *via* ^1H NMR, FTIR, and UV-Vis spectroscopy, which demonstrated major effects on the cell performance.¹¹⁰ Notably, glyme-based electrolytes would also ensure a wide temperature range of applicability, as demonstrated in a further report. As expected, the polarization and rate capability of a $\text{Li}-\text{O}_2$ cell using $\text{G}_4\text{-LiTf}$ were shown to be influenced by the operating temperature (Fig. 8c). Indeed, low temperatures would slow down the diffusion of Li^+ ions, whilst elevated temperatures would decrease the electrolyte viscosity and consequently increase the oxygen mobility. Thermal effects on the crystallinity of Li_2O_2 formed upon cell discharging were also observed.¹¹¹ It is worth considering that the reversibility of the $\text{Li}-\text{O}_2$ process upon full-capacity cycling is rather poor, and the outstanding long-term performances reported so far have been often obtained by limiting the capacity below 1000 mA h

$\text{g}_{\text{carbon}}^{-1}$. On the other hand, it has been demonstrated that extended full-capacity cycling of $\text{Li}-\text{O}_2$ batteries using glymes would be ensured by selecting appropriate electrode materials (carbon source and catalyst) and cycling protocols. In particular, the formation of a stable interfacial layer on the cathode surface during the initial cycling may stabilize the subsequent cycling stages. Whilst the initial cell operation was characterized by the predominant formation of Li_2O_2 , the subsequent cycles led to the predominant formation of side products and the eventual stabilization of the yield of Li_2O_2 at about 33–40%.¹¹² Besides, interesting results have been obtained by limiting the capacity of a $\text{Li}-\text{O}_2$ battery to 1000 mA h $\text{g}_{\text{carbon}}^{-1}$ using an electrolyte with very low volatility. The electrolyte was formed by dissolving LiTFSI in PEGDME (MW 500 g mol⁻¹) and then mixing this solution with the $\text{Pyr}_{14}\text{TFSI}$ ionic liquid.¹¹³ Moreover, a new lithium-ether-derived chelate IL showed promising characteristics for applications in $\text{Li}-\text{O}_2$ batteries, namely, high stability against the lithium metal anode and against superoxide-initiated hydrogen abstraction when compared to DME. This electrolyte chemistry ensured a decrease in the amount of parasitic species formed during cycling, such as formate, as well as a ten-fold decrease in CO_2 evolution upon charge as compared to that observed in DME-based solutions.¹¹⁴ Among the various possible lithium salts for aprotic solutions for $\text{Li}-\text{O}_2$ batteries, LiNO_3 dissolved in polyether solvents exhibited beneficial properties on both the ORR and OER. The anion enhanced the former reaction by enabling the formation of submicrometric Li_2O_2 particles *via* a reaction pathway involving superoxide radicals and acted as a redox mediator by producing at the negative electrode NO_2^- ions which, in turn, formed NO_2 at 3.6–3.8 V *vs.* Li^+/Li . This latter species catalyze the Li_2O_2 oxidation forming NO_2^- , which is then oxidized again, thereby decreasing the OER overpotentials within the electrochemical stability window of glyme-based electrolytes.¹¹⁵ 1 M solutions of LiTf, LiTFSI, and LiFSI in G_4 were further studied in $\text{Li}-\text{O}_2$ batteries to elucidate the interplay between ion transport and lithium stripping/plating, thereby revealing for the $\text{G}_4\text{-LiTFSI}$ electrolyte mixture a high rate capability, a fast electrochemical reaction at the anode side, and a promising performance. Notably, the performance of the $\text{Li}-\text{O}_2$ cell depended on lithium oxide layers formed on the negative electrode. These results suggested that a suitable anode-surface oxidation may enhance the electrode/electrolyte interface characteristics.^{116,120} The electrolyte formulation and the electrochemical conditions may affect both kinetics and thermodynamics of the ORR, for instance by altering the solvation in high DN solvents. Along with solvent DN, the level of dissociation of the salt may have additional contributions in determining the characteristics of the ORR and controlling the morphology of Li_2O_2 deposits, as schematically illustrated in Fig. 8d.¹¹⁷ Besides fundamental studies aiming to shed light on the electrochemical reactions occurring in the cell, further works focused on developing alternative battery designs, such as the metal-free Li-ion oxygen system which was mentioned above. For example, an effective approach to achieve excellent cycling stability and low cell polarization over



100 cycles involved the use of silicon particles at the negative electrode. In this regard, a stable SEI over the anode surface would mitigate oxygen crossover effects, which would improve the long-term cyclability of the battery.¹¹⁸ Another lithium-ion oxygen cell using a lithiated hard carbon (HC) anode, a monolithic carbon cathode, and a G₂-based electrolyte was reported with promising results.¹²¹ Additional evidence of the role played by the anion nature in the amount of Li₂O₂ precipitated on the separator in the Li–O₂ cell using glyme-based electrolytes suggested a relationship between the stability of the discharge intermediate (LiO₂) in the electrolyte and the anion. Accordingly, electrolyte solutions characterized by a high intermediate solubility would favor the precipitation of Li₂O₂ across the cell, thereby adversely affecting the reversibility of the oxygen conversion process. Fig. 8e shows how the fraction of Li₂O₂ in the separator, with reference to the theoretical total amount of Li₂O₂, changes with the anion composition.¹¹⁹

As discussed in the previous sections, literature reports have described various beneficial properties of SILs when compared to conventional electrolytes for applications in lithium batteries employing insertion and sulfur-conversion cathodes. SILs may improve the Li–O₂ cell too, as demonstrated by a study of G₃–LiTFSI mixtures where the solvent and salts were in an equimolar ratio or contained excess glyme. The related results suggested that SILs would have a higher oxidative stability than conventional electrolytes, as well as a lower volatility, which would suit the open Li–O₂ cell configuration. High salt concentrations would mitigate the parasitic reactions that lead to CO₂ evolution, as shown in Fig. 8f, although either type of solution did not ensure the full theoretical value of O₂ evolution, and side processes were detected upon charging. The discharge product morphology was also related to the solubility of the superoxide intermediate, which is in turn affected by the salt concentration.¹²² Moreover, Raman spectroscopy analyses of glyme-based electrolytes suggested that the increase in LiTFSI concentration favors the formation of cationic and anionic complexes that stabilize the G₄ molecules against degradation. High-concentration electrolytes enabled an improvement as high as 300% in charge/discharge cycling tests with a limited capacity of 500 mA h g^{−1}, for solutions containing higher LiTFSI concentrations. A better cyclability at a low G₄ : LiTFSI molar ratio was associated with a decrease in the growth rate of lithium carbonate species deriving from glyme degradation.¹²³ On the other hand, a G₄–LiTFSI solution with a 1 mol kg^{−1} concentration enabled the achievement of hundreds of cycles without signs of decay to a Li–O₂ cell using a multiwalled carbon nanotube electrode. The reversibility of the electrochemical process in this cell was demonstrated by detecting the reversible formation and dissolution of Li₂O₂ during the electrochemical process.¹²⁴ Regarding this point, the Li₂O₂ oxidation pathway was associated with the solvent donicity according to a strong solvent-controlled mechanism. Thus, a solution route forming a soluble LiO₂ intermediate after Li₂O₂ oxidation was suggested to occur in high-donicity solvents (Fig. 8g, right-hand side pathway), whilst a solid-solution route forming a solid Li_{2-x}O₂ intermediate was identified

in low-donicity solvents (Fig. 8g, left-hand side pathway). Notably, the former oxidation mechanism was causally related to an observed poor cycling stability of the relevant Li–O₂ cells.¹²⁵ A key aspect to consider when increasing the salt concentration in G_n–LiX solutions is the change in Li⁺ transport properties and ionic conductivity, as indeed extensively discussed in section 4. We remark herein that viscosity and Li⁺ transference number measurements on solutions using either G₁ or G₂ and either LiTf or LiTFSI suggested a failure of Walden's rule, in spite of a qualitative correlation with the association constant of the salts.¹²⁶

The electrolyte composition may affect the crucial parameters for application in a Li–O₂ battery using a carbon-cloth GDL, such as the conductivity, viscosity, contact angle, and decomposition temperature. Among various formulations, G₄–LiTFSI was often selected as the electrolyte of choice due to its suitable properties for use in the open metal–oxygen cell design. In this regard, a recent work demonstrated an enhanced performance as compared to those obtained with other formulations, that is, a longer cycle life at a discharge capacity limit of 2000 mA h g^{−1} with reference to the mass of the Pt catalyst in the GDL.¹²⁷ As mentioned above, LiNO₃-based solutions have been investigated as electrolytes for Li–O₂ batteries with promising results, which were attributed to the role of NO₃[−] as a redox mediator for the electrochemical process. Furthermore, LiNO₃ was shown to improve the lithium–electrolyte interphase by favoring the formation of a Li₂O layer which mitigates the lithium dendrite growth and the electrolyte decomposition. Dual solvent systems based on DMSO and G₄ were suggested as effective solutions characterized by an increased number per volume and mobility of Li⁺ and NO₃[−]. The former solvent has a relatively high dielectric constant and a low viscosity, which allowed a decrease in the overpotential of the charge process along with an enhancement of the power density of the battery. Such a mixed formulation mitigated the low dissociation degree of LiNO₃ typically leading to low ionic conductivity.¹²⁸ As for the effects of the glyme chain length, SNIFTIRS and electrochemical data on Li–O₂ cells using gold electrodes lately suggested that G₂ may be more stable than G₄ between 3.6 and 3.9 V vs. Li⁺/Li, although water impurities may reduce its stability.¹²⁹ On the other hand, a recent comparative study of concentrated solutions of LiTFSI and LiNO₃ salts in either G₂ or G₃ demonstrated that the former solvent would have volatility issues limiting its applicability in Li–O₂ cells with open design. Gradual solvent evaporation during cycling was observed along with a rapid cell failure. In contrast, the use of the G₃-based electrolyte ensured stability over time as well as a specific capacity ranging from 500 to 1000 mA h g_{carbon}^{−1}. Such a concentrated G₃–LiTFSI–LiNO₃ was characterized by a high conductivity, a high Li⁺ transference number, a wide electrochemical stability window, and favorable lithium–metal passivation properties.¹³⁰

Despite still being in a very early stage, the Li–O₂ battery is the most appealing energy storage system due to the highest theoretical potentialities among the various candidates. Parasitic reaction of the electrolyte solvents with the radicals



formed during the Li–O₂ electrochemical process as well as the necessity of operating in an open environment (*i.e.*, O₂ or dry air) represent the major drawbacks to overcome for enabling an efficient battery. Glyme electrolytes, which are modulable in terms of stability and volatility by changing the chain length, as well as the salt nature and concentration represent the most suitable electrolyte for allowing cell operation. Furthermore, the use of the lithium metal in a practical battery exposed to oxygen or air may be actually granted by long chain glymes such as highly viscous or solid PEGDME. In this regard, alternative lithium metal-free batteries are proposed in analogy with the Li-ion ones by using alloying electrodes at the negative side, however with partial success. A solution based on G₄ represents the first reported example of an electrolyte in a lithium oxygen cell with high capacity and a stable trend. G₃ may be also adequate for Li–O₂ cells, but G₂ and G₁ appear unsuitable at the moment due to excessive volatility, and consequent evaporation during cell cycling in an open environment. The salt-to-solvent molar ratio is crucial for the lithium–oxygen conversion mechanism: indeed, intermediate concentrations limit the glyme decomposition due to O₂^{•-} radicals, but low concentrations lead to detrimental decomposition. Decomposition reaction is in fact governed by the intermediate Li⁺(G_n)O₂^{•-} complex which can form coordinated Li⁺ ions, CIP, SSIP solvates, and free glyme molecules. The latter species are principally formed at low concentrations and can react with O₂^{•-}, thus leading to the electrolyte decomposition. In addition, solvent chemistry controls the reaction mechanism: solvents with high DN lead to the formation of a soluble LiO₂ intermediate, but solvents with low DN favor the formation of a Li_{2-x}O₂ intermediate through a solid-solution mechanism. It is worth mentioning that the performances of the Li–O₂ cell are also affected by the temperature, the use of adequate GDLs, the cell setup and the experimental conditions, as well by the presence of LiNO₃ even though with less remarkable effects compared to Li–S batteries. Furthermore, SIL formation may improve the Li–O₂ battery performance, while high salt concentration can mitigate the parasitic reactions due to the formation of cationic and anionic complexes, particularly using G₄.

7. Remarks and conclusions

Extensive works have been conducted over the past 25 years to assess the possible applicability of glymes in lithium batteries and shed light on the chemical–physical properties of their mixtures with lithium salts. Indeed, the various advantages of glyme-based electrolytes against common alkyl-carbonate-based solutions have been often highlighted, although some questions on their high-power performance when compared to their conventional, ester-based counterpart are still open. So far, glyme-based solutions have been thoroughly studied by using a wide portfolio of experimental methods, modelling approaches, and techniques, which have provided comprehensive description of their highly versatile characteristics,

tunable by changing the glyme chain length along with the salt composition and concentration. Notably, glyme-based solutions typically exhibit a higher thermal stability as well as lower flammability and volatility than common lithium-battery electrolytes, particularly at middle and moderately high chain lengths, thereby possibly enabling the use of the high-energy lithium–metal anode. Thanks to such tailored properties, glymes can be effectively employed in lithium batteries with insertion cathodes working below 4 V, such as LiFePO₄, as well as with 4 V-class cathodes such as LiCoO₂, NMC and LiMn_xFe_{1-x}PO₄ when used in concentrated formulations as salt-in-solvent mixtures or SILs. Furthermore, glymes are especially suited for high-energy Li–S batteries and considered to be the solvents of choice for Li–O₂ batteries, due to a high chemical stability in the cell along with a suitable volatility for the open design. Among the various lithium salts for glyme-based electrolytes that have been investigated, LiTFSI, LiTf, LiFSI, and LiBETI have shown favorable characteristics in the above-mentioned cell designs based on insertion or conversion chemistries. Furthermore, the crucial role of LiNO₃ as a film-forming additive to achieve reversible lithium–metal plating and anode protection in conventional Li–metal and Li–S batteries has been clearly demonstrated, and its additional redox-mediator properties in Li–O₂ cells have been suggested.

Interestingly, the electrolyte properties may vary between an SIL and a conventional electrolyte, depending on the concentration and nature of the salt, along with the glyme chain length. As extensively discussed in the previous sections, an SIL has been described as a [Li(G_n)]X system, where Li⁺ is mainly solvated by crown-ether-like curled G_n molecules forming a complex in contact with the TFSI[–] anion, and negligible “free” solvent is detected in the mixture. In this regard, the stability of the [Li(G_n)]⁺ complex may be revealed by comparing the ratio between the self-diffusion coefficients of glyme and Li⁺ ions (D_G/D_{Li}). Therefore, when designing a high-concentration glyme-based electrolyte, the peculiar features of the anion should be considered along with the solvent molecular weight. As an example, we remark that TFSI[–] would favor the formation of SILs, whilst TDI[–] would promote ionic aggregation. Herein, we point out that the Li⁺ transference number of SILs under anion-blocking conditions is typically low because of the Li⁺–G_n complexation, which causes anti-correlation of cation and anion motion due to momentum conservation. In contrast, conventional concentrated solutions exhibit momentum exchange between ions and solvent molecules. Strong Lewis base anions ensure collective migration of ion pairs, which leads to a high Li⁺ transference number and a low ionic conductivity. Instead, anions with low Lewis basicity typically lead to a high conductivity and a low Li⁺ transference number. The increase in viscosity might be another drawback of highly concentrated G_n–LiX mixtures, which may require the use of diluents to increase the ionic conductivity. Lithium dendrite formation and anode passivation properties are other key aspects to consider when optimizing an electrolyte formulation enhanced by additives.



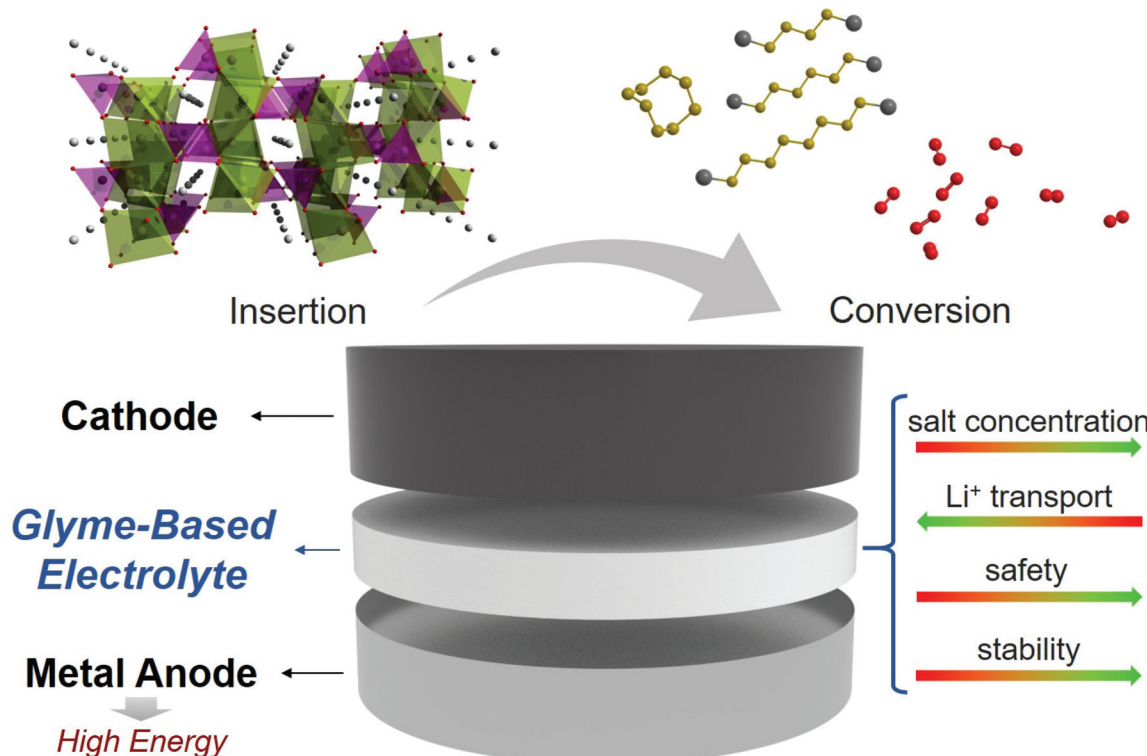


Fig. 9 Schematic representation of the promising characteristics of glyme-based electrolyte solutions for application in lithium–metal batteries using insertion (e.g., olivine-based compounds) as well as conversion cathodes (e.g., S-based and O₂-based electrodes); the typical relationship between LiX salt concentration, Li⁺ transport properties, safety, and stability of the glyme-based solutions is also shown.

Several works have suggested that SILs may improve the long-term cycling ability of Li–S cells by preventing the shuttle effect. According to this approach, the polysulfide dissolution would be significantly decreased by limiting the amount of “free” solvent molecules able to participate in the solvation process, thereby leading to a quasi-solid sulfur reaction mechanism in the cell. On the other hand, glyme-based cathodes have shown a promising performance in a wide range of current rates, benefiting from a highly reversible polysulfide conversion on the positive electrode and from suitable Li⁺ transport properties. Concerning this point, the addition of LiNO₃ to the glyme-based electrolyte can actually mitigate the detrimental reaction of dissolved polysulfide with lithium by enabling efficient protection of the metal anode against this parasitic process. As for the Li–O₂ system, the electrolyte formulation controls the Li–O₂ conversion mechanism and the morphology of the Li₂O₂ discharge product, thus influencing the cell performance. Indeed, solvent DN and dissociation level of the salt may drive the pathway of the ORR. Moreover, literature works have suggested favorable properties of SILs compared to conventional electrolyte solutions.

Fig. 9 summarizes the main concepts discussed herein and the main conclusions drawn by reviewing the most relevant studies of glyme-based electrolytes for lithium batteries. The figure shows that the glyme-based electrolytes can allow the change from the intercalation chemistry to the more energetic

and alternative conversion chemistry (top-side scheme) and the use of the lithium metal in batteries (bottom-side scheme). In particular, PEGDME in the liquid and solid states is non-toxic, nonflammable, and safe and can actually allow scalable Li–S and Li–O₂ batteries for future applications. Fig. 9 also reveals that the increase of the salt concentration in the glyme-based electrolytes unlikely leads to the decrease of the lithium transference number; however it increases at the same time the safety and stability of the battery (right-hand arrows). In this scenario the electrolyte viscosity may potentially represent advantages in terms of scalability, and disadvantages in terms of conductivity and cell performances. The fundamental investigation and applied research have indeed enabled a deep understanding of the G_n–LiX structure along with substantial technological improvements of the lithium cell. A critical analysis of the extensive experimental evidence collected over the last two decades demonstrates the suitability of glymes as electrolyte solvents for lithium–metal batteries, and suggests viable strategies to achieve enhanced, next-generation energy-storage systems.

Conflicts of interest

The authors declare no conflicts of interest.

Acknowledgements

This project/work has received funding from the European Union's Horizon 2020 research and innovation programme Graphene Flagship under grant agreement no. 881603. The authors are also thankful for the grant "Fondo di Ateneo per la Ricerca Locale (FAR) 2021", University of Ferrara, and the Institute of Global Innovation Research (GIR) in Tokyo University of Agriculture and Technology.

Notes and references

- 1 P. Jessop, *Green Chem.*, 2020, **22**, 13–15.
- 2 D. Di Lecce, R. Verrelli and J. Hassoun, *Green Chem.*, 2017, **19**, 3442–3467.
- 3 M. Marinaro, D. Bresser, E. Beyer, P. Faguy, K. Hosoi, H. Li, J. Sakovica, K. Amine, M. Wohlfahrt-Mehrens and S. Passerini, *J. Power Sources*, 2020, **459**, 228073.
- 4 A. A. Kebede, T. Coosemans, M. Messagie, T. Jemal, H. A. Behabtu, J. Van Mierlo and M. Berecibar, *J. Energy Storage*, 2021, **40**, 102748.
- 5 T. Chen, Y. Jin, H. Lv, A. Yang, M. Liu, B. Chen, Y. Xie and Q. Chen, *Trans. Tianjin Univ.*, 2020, **26**, 208–217.
- 6 A. Varzi, K. Thanner, R. Scipioni, D. Di Lecce, J. Hassoun, S. Dörfler, H. Altheus, S. Kaskel, C. Prehal and S. A. Freunberger, *J. Power Sources*, 2020, **480**, 228803.
- 7 K. Xu, *Chem. Rev.*, 2014, **114**, 11503–11618.
- 8 Y. Zhang, T.-T. Zuo, J. Popovic, K. Lim, Y.-X. Yin, J. Maier and Y.-G. Guo, *Mater. Today*, 2020, **33**, 56–74.
- 9 K. Qin, K. Holguin, M. Mohammadiroobbari, J. Huang, E. Y. S. Kim, R. Hall and C. Luo, *Adv. Funct. Mater.*, 2021, **31**, 2009694.
- 10 X. He, D. Bresser, S. Passerini, F. Baakes, U. Krewer, J. Lopez, C. T. Mallia, Y. Shao-Horn, I. Cekic-Laskovic, S. Wiemers-Meyer, F. A. Soto, V. Ponce, J. M. Seminario, P. B. Balbuena, H. Jia, W. Xu, Y. Xu, C. Wang, B. Horstmann, R. Amine, C.-C. Su, J. Shi, K. Amine, M. Winter, A. Latz and R. Kostecki, *Nat. Rev. Mater.*, 2021, **6**, 1036–1052.
- 11 M. Ue and K. Uosaki, *Curr. Opin. Electrochem.*, 2019, **17**, 106–113.
- 12 D. Campanella, D. Belanger and A. Paoletta, *J. Power Sources*, 2021, **482**, 228949.
- 13 K. Liu, Z. Wang, L. Shi, S. Jungsuttiwong and S. Yuan, *J. Energy Chem.*, 2021, **59**, 320–333.
- 14 I. Osada, H. De Vries, B. Scrosati and S. Passerini, *Angew. Chem., Int. Ed.*, 2016, **55**, 500–513.
- 15 P. Ding, Z. Lin, X. Guo, L. Wu, Y. Wang, H. Guo, L. Li and H. Yu, *Mater. Today*, 2021, **51**, 449–474.
- 16 D. Aurbach and E. Granot, *Electrochim. Acta*, 1997, **42**, 697–718.
- 17 D. Brouillet, G. Perron and J. E. Desnoyers, *J. Solution Chem.*, 1998, **27**, 151–182.
- 18 D. Brouillet, D. E. Irish, N. J. Taylor, G. Perron, M. Odziemkowski and J. E. Desnoyers, *Phys. Chem. Chem. Phys.*, 2002, **4**, 6063–6071.
- 19 S. Tobishima, H. Morimoto, M. Aoki, Y. Saito, T. Inose, T. Fukumoto and T. Kuryu, *Electrochim. Acta*, 2004, **49**, 979–987.
- 20 W. A. Henderson, F. McKenna, M. A. Khan, N. R. Brooks, V. G. Young and R. Frech, *Chem. Mater.*, 2005, **17**, 2284–2289.
- 21 W. A. Henderson, *J. Phys. Chem. B*, 2006, **110**, 13177–13183.
- 22 C. Zhang, D. Ainsworth, Y. G. Andreev and P. G. Bruce, *J. Am. Chem. Soc.*, 2007, **129**, 8700–8701.
- 23 A. Plewa, M. Kalita and M. Siekierski, *Electrochim. Acta*, 2007, **53**, 1527–1534.
- 24 A. Plewa-Marczewska, M. Kalita, M. Marczewski and M. Siekierski, *Electrochim. Acta*, 2010, **55**, 1389–1395.
- 25 S. Tang and H. Zhao, *RSC Adv.*, 2014, **4**, 11251.
- 26 A.-A. G. Shaikh and S. Sivaram, *Chem. Rev.*, 1996, **96**, 951–976.
- 27 F. Guo, W. Hase, Y. Ozaki, Y. Konno, M. Inatsuki, K. Nishimura, N. Hashimoto and O. Fujita, *Exp. Therm. Fluid Sci.*, 2019, **109**, 109858.
- 28 B. Schäffner, F. Schäffner, S. P. Verevkin and A. Börner, *Chem. Rev.*, 2010, **110**, 4554–4581.
- 29 E. R. Logan, E. M. Tonita, K. L. Gering, L. Ma, M. K. G. Bauer, J. Li, L. Y. Beaulieu and J. R. Dahn, *J. Electrochem. Soc.*, 2018, **165**, A705–A716.
- 30 A. Conesa, S. Shen and A. Coronas, *Int. J. Thermophys.*, 1998, **19**, 1343–1358.
- 31 K. Schoenhammer, H. Petersen, F. Guethlein and A. Goepferich, *Pharm. Res.*, 2009, **26**, 2568–2577.
- 32 J. Kalhoff, G. G. Eshetu, D. Bresser and S. Passerini, *ChemSusChem*, 2015, **8**, 2154–2175.
- 33 S. Zhang, K. Ueno, K. Dokko and M. Watanabe, *Adv. Energy Mater.*, 2015, **5**, 1500117.
- 34 R. Gond, W. van Ekeren, R. Mogensen, A. J. Naylor and R. Younesi, *Mater. Horiz.*, 2021, **8**, 2913–2928.
- 35 Y. Liu, S. Fang, P. Shi, D. Luo, L. Yang and S. Hirano, *J. Power Sources*, 2016, **331**, 445–451.
- 36 S. Li, F. Lorandi, H. Wang, T. Liu, J. F. Whitacre and K. Matyjaszewski, *Prog. Polym. Sci.*, 2021, **122**, 101453.
- 37 F. Croce, G. B. Appetecchi, L. Persi and B. Scrosati, *Nature*, 1998, **394**, 456–458.
- 38 Y. H. Jo, S. Li, C. Zuo, Y. Zhang, H. Gan, S. Li, L. Yu, D. He, X. Xie and Z. Xue, *Macromolecules*, 2020, **53**, 1024–1032.
- 39 X.-L. Wang, A. Mei, X.-L. Li, Y.-H. Lin and C.-W. Nan, *J. Power Sources*, 2007, **171**, 913–916.
- 40 G. Derrien, J. Hassoun, S. Sacchetti and S. Panero, *Solid State Ionics*, 2009, **180**, 1267–1271.
- 41 S. Li, F. Lorandi, J. F. Whitacre and K. Matyjaszewski, *Macromol. Chem. Phys.*, 2020, **221**, 1900379.
- 42 C. Li, S. Liu, C. Shi, G. Liang, Z. Lu, R. Fu and D. Wu, *Nat. Commun.*, 2019, **10**, 1363.
- 43 T. Tamura, T. Hachida, K. Yoshida, N. Tachikawa, K. Dokko and M. Watanabe, *J. Power Sources*, 2010, **195**, 6095–6100.
- 44 A. Orita, K. Kamijima, M. Yoshida, K. Dokko and M. Watanabe, *J. Power Sources*, 2011, **196**, 3874–3880.



45 S. Seki, K. Takei, H. Miyashiro and M. Watanabe, *J. Electrochem. Soc.*, 2011, **158**, A769.

46 K. Yoshida, M. Nakamura, Y. Kazue, N. Tachikawa, S. Tsuzuki, S. Seki, K. Dokko and M. Watanabe, *J. Am. Chem. Soc.*, 2011, **133**, 13121–13129.

47 K. Yoshida, M. Tsuchiya, N. Tachikawa, K. Dokko and M. Watanabe, *J. Electrochem. Soc.*, 2012, **159**, A1005–A1012.

48 S. Seki, N. Serizawa, K. Takei, K. Dokko and M. Watanabe, *J. Power Sources*, 2013, **243**, 323–327.

49 N. Serizawa, S. Seki, K. Takei, H. Miyashiro, K. Yoshida, K. Ueno, N. Tachikawa, K. Dokko, Y. Katayama, M. Watanabe and T. Miura, *J. Electrochem. Soc.*, 2013, **160**, A1529–A1533.

50 C. Zhang, A. Yamazaki, J. Murai, J.-W. Park, T. Mandai, K. Ueno, K. Dokko and M. Watanabe, *J. Phys. Chem. C*, 2014, **118**, 17362–17373.

51 H. Hirayama, N. Tachikawa, K. Yoshii, M. Watanabe and Y. Katayama, *Electrochemistry*, 2015, **83**, 824–827.

52 Y. Gambe, Y. Sun and I. Honma, *Sci. Rep.*, 2015, **5**, 8869.

53 D. Di Lecce, L. Carbone, V. Gancitano and J. Hassoun, *J. Power Sources*, 2016, **334**, 146–153.

54 L. Carbone, M. Gobet, J. Peng, M. Devany, B. Scrosati, S. Greenbaum and J. Hassoun, *J. Power Sources*, 2015, **299**, 460–464.

55 L. Carbone, D. Di Lecce, M. Gobet, S. Munoz, M. Devany, S. Greenbaum and J. Hassoun, *ACS Appl. Mater. Interfaces*, 2017, **9**, 17085–17095.

56 D. Shanmukaraj, S. Lois, S. Fantini, F. Malbosc and M. Armand, *Chem. Mater.*, 2018, **30**, 246–251.

57 S. Wei, Z. Li, K. Kimura, S. Inoue, L. Pandini, D. Di Lecce, Y. Tominaga and J. Hassoun, *Electrochim. Acta*, 2019, **306**, 85–95.

58 V. Marangon, Y. Tominaga and J. Hassoun, *J. Power Sources*, 2020, **449**, 227508.

59 S. Wei, S. Inoue, D. di Lecce, Z. Li, Y. Tominaga and J. Hassoun, *ChemElectroChem*, 2020, **7**, 2344–2344.

60 V. Marangon, L. Minnetti, M. Adami, A. Barlini and J. Hassoun, *Energy Fuels*, 2021, **35**, 10284–10292.

61 S. Terada, K. Ikeda, K. Ueno, K. Dokko and M. Watanabe, *Aust. J. Chem.*, 2019, **72**, 70.

62 K. Ueno, R. Tatara, S. Tsuzuki, S. Saito, H. Doi, K. Yoshida, T. Mandai, M. Matsugami, Y. Umebayashi, K. Dokko and M. Watanabe, *Phys. Chem. Chem. Phys.*, 2015, **17**, 8248–8257.

63 R. Kido, K. Ueno, K. Iwata, Y. Kitazawa, S. Imaizumi, T. Mandai, K. Dokko and M. Watanabe, *Electrochim. Acta*, 2015, **175**, 5–12.

64 L. Aguilera, S. Xiong, J. Scheers and A. Matic, *J. Mol. Liq.*, 2015, **210**, 238–242.

65 S. Seki, N. Serizawa, K. Takei, S. Tsuzuki, Y. Umebayashi, Y. Katayama, T. Miura, K. Dokko and M. Watanabe, *RSC Adv.*, 2016, **6**, 33043–33047.

66 S. Saito, H. Watanabe, K. Ueno, T. Mandai, S. Seki, S. Tsuzuki, Y. Kameda, K. Dokko, M. Watanabe and Y. Umebayashi, *J. Phys. Chem. B*, 2016, **120**, 3378–3387.

67 K. Ueno, J. Murai, K. Ikeda, S. Tsuzuki, M. Tsuchiya, R. Tatara, T. Mandai, Y. Umebayashi, K. Dokko and M. Watanabe, *J. Phys. Chem. C*, 2016, **120**, 15792–15802.

68 J. Peng, L. Carbone, M. Gobet, J. Hassoun, M. Devany and S. Greenbaum, *Electrochim. Acta*, 2016, **213**, 606–612.

69 M. Callsen, K. Sodeyama, Z. Futera, Y. Tateyama and I. Hamada, *J. Phys. Chem. B*, 2017, **121**, 180–188.

70 P. Jankowski, M. Dranka, W. Wieczorek and P. Johansson, *J. Phys. Chem. Lett.*, 2017, **8**, 3678–3682.

71 K. Hayamizu, *Electrochim. Acta*, 2017, **254**, 101–111.

72 M. Saito, S. Yamada, T. Ishikawa, H. Otsuka, K. Ito and Y. Kubo, *RSC Adv.*, 2017, **7**, 49031–49040.

73 D. Dong, F. Sälzer, B. Roling and D. Bedrov, *Phys. Chem. Chem. Phys.*, 2018, **20**, 29174–29183.

74 J. Popovic, D. Höfler, J. P. Melchior, A. Münchinger, B. List and J. Maier, *J. Phys. Chem. Lett.*, 2018, **9**, 5116–5120.

75 Y. Sun and I. Hamada, *J. Phys. Chem. B*, 2018, **122**, 10014–10022.

76 M. Nojabaei, J. Popovic and J. Maier, *J. Mater. Chem. A*, 2019, **7**, 13331–13338.

77 J.-D. Xie, W.-J. Liu, C. Li, J. Patra, Y. A. Gandomi, Q.-F. Dong and J.-K. Chang, *Electrochim. Acta*, 2019, **319**, 625–633.

78 N. Arai, H. Watanabe, T. Yamaguchi, S. Seki, K. Ueno, K. Dokko, M. Watanabe, Y. Kameda, R. Buchner and Y. Umebayashi, *J. Phys. Chem. C*, 2019, **123**, 30228–30233.

79 F. Schmidt and M. Schönhoff, *J. Phys. Chem. B*, 2020, **124**, 1245–1252.

80 N. Arai, H. Watanabe, E. Nozaki, S. Seki, S. Tsuzuki, K. Ueno, K. Dokko, M. Watanabe, Y. Kameda and Y. Umebayashi, *J. Phys. Chem. Lett.*, 2020, **11**, 4517–4523.

81 K. Shigenobu, K. Dokko, M. Watanabe and K. Ueno, *Phys. Chem. Chem. Phys.*, 2020, **22**, 15214–15221.

82 K. Shigenobu, M. Shibata, K. Dokko, M. Watanabe, K. Fujii and K. Ueno, *Phys. Chem. Chem. Phys.*, 2021, **23**, 2622–2629.

83 J. Kim, J. Hassoun, S. Panero, Y. K. Sun and B. Scrosati, *Green*, 2011, **1**, 323–328.

84 K. Dokko, N. Tachikawa, K. Yamauchi, M. Tsuchiya, A. Yamazaki, E. Takashima, J.-W. Park, K. Ueno, S. Seki, N. Serizawa and M. Watanabe, *J. Electrochem. Soc.*, 2013, **160**, A1304–A1310.

85 K. Ueno, J.-W. Park, A. Yamazaki, T. Mandai, N. Tachikawa, K. Dokko and M. Watanabe, *J. Phys. Chem. C*, 2013, **117**, 20509–20516.

86 L. Carbone, M. Gobet, J. Peng, M. Devany, B. Scrosati, S. Greenbaum and J. Hassoun, *ACS Appl. Mater. Interfaces*, 2015, **7**, 13859–13865.

87 M. Cuisinier, C. Hart, M. Balasubramanian, A. Garsuch and L. F. Nazar, *Adv. Energy Mater.*, 2015, **5**, 1401801.

88 M. Agostini, S. Xiong, A. Matic and J. Hassoun, *Chem. Mater.*, 2015, **27**, 4604–4611.

89 C. Li, A. L. Ward, S. E. Doris, T. A. Pascal, D. Prendergast and B. A. Helms, *Nano Lett.*, 2015, **15**, 5724–5729.

90 H. Lu, Y. Yuan, Z. Hou, Y. Lai, K. Zhang and Y. Liu, *RSC Adv.*, 2016, **6**, 18186–18190.



91 K. Ueno, *Electrochemistry*, 2016, **84**, 674–680.

92 L. Carbone, J. Peng, M. Agostini, M. Gobet, M. Devany, B. Scrosati, S. Greenbaum and J. Hassoun, *ChemElectroChem*, 2017, **4**, 209–215.

93 S. Usuki, S. Uchida, Y. Matsui, M. Yamagata, H. Hinago and M. Ishikawa, *Electrochemistry*, 2017, **85**, 650–655.

94 S. Seki, N. Serizawa, K. Takei, Y. Umebayashi, S. Tsuzuki and M. Watanabe, *Electrochemistry*, 2017, **85**, 680–682.

95 Q. Zhang, D. C. Bock, K. J. Takeuchi, A. C. Marschilok and E. S. Takeuchi, *J. Electrochem. Soc.*, 2017, **164**, A897–A901.

96 S. Okabe, S. Uchida, Y. Matsui, M. Yamagata and M. Ishikawa, *Electrochemistry*, 2017, **85**, 671–674.

97 M. Haruta, T. Moriyasu, A. Tomita, T. Takenaka, T. Doi and M. Inaba, *J. Electrochem. Soc.*, 2018, **165**, A1874–A1879.

98 Y. Ishino, K. Takahashi, W. Murata, Y. Umebayashi, S. Tsuzuki, M. Watanabe, M. Kamaya and S. Seki, *Energy Technol.*, 2019, **7**, 1900197.

99 D. Di Lecce, V. Marangon, A. Benítez, Á. Caballero, J. Morales, E. Rodríguez-Castellón and J. Hassoun, *J. Power Sources*, 2019, **412**, 575–585.

100 A. Gupta, A. Bhargav, J.-P. Jones, R. V. Bugga and A. Manthiram, *Chem. Mater.*, 2020, **32**, 2070–2077.

101 U. Košir, I. K. Cigić, J. Markelj, S. D. Talian and R. Dominko, *Electrochim. Acta*, 2020, **363**, 137227.

102 M. Nojabaei, K. Küster, U. Starke, J. Popovic and J. Maier, *Small*, 2020, **16**, 2000756.

103 S. Dörfler, H. Althues, P. Härtel, T. Abendroth, B. Schumm and S. Kaskel, *Joule*, 2020, **4**, 539–554.

104 V. Marangon, D. di Lecce, L. Minnetti and J. Hassoun, *ChemElectroChem*, 2021, **8**, 3971–3981.

105 J. Hassoun, F. Croce, M. Armand and B. Scrosati, *Angew. Chem. – Int. Ed.*, 2011, **50**, 2999–3002.

106 H. G. Jung, J. Hassoun, J. B. Park, Y. K. Sun and B. Scrosati, *Nat. Chem.*, 2012, **4**, 579–585.

107 W. Xu, J. Hu, M. H. Engelhard, S. A. Towne, J. S. Hardy, J. Xiao, J. Feng, M. Y. Hu, J. Zhang, F. Ding, M. E. Gross and J. G. Zhang, *J. Power Sources*, 2012, **215**, 240–247.

108 J. Hassoun, H.-G. Jung, D.-J. Lee, J.-B. Park, K. Amine, Y.-K. Sun and B. Scrosati, *Nano Lett.*, 2012, **12**, 5775–5779.

109 F. Li, T. Zhang, Y. Yamada, A. Yamada and H. Zhou, *Adv. Energy Mater.*, 2013, **3**, 532–538.

110 K. U. Schwenke, S. Meini, X. Wu, H. A. Gasteiger and M. Piana, *Phys. Chem. Chem. Phys.*, 2013, **15**, 11830.

111 J. B. Park, J. Hassoun, H. G. Jung, H. S. Kim, C. S. Yoon, I. H. Oh, B. Scrosati and Y. K. Sun, *Nano Lett.*, 2013, **13**, 2971–2975.

112 E. N. Nasybulin, W. Xu, B. L. Mehdi, E. Thomsen, M. H. Engelhard, R. C. Massé, P. Bhattacharya, M. Gu, W. Bennett, Z. Nie, C. Wang, N. D. Browning and J.-G. Zhang, *ACS Appl. Mater. Interfaces*, 2014, **6**, 14141–14151.

113 G. A. Elia, R. Bernhard and J. Hassoun, *RSC Adv.*, 2015, **5**, 21360–21365.

114 B. D. Adams, R. Black, Z. Williams, R. Fernandes, M. Cuisinier, E. J. Berg, P. Novak, G. K. Murphy and L. F. Nazar, *Adv. Energy Mater.*, 2015, **5**, 1400867.

115 D. Sharon, D. Hirsberg, M. Afri, F. Chesneau, R. Lavi, A. a. Frimer, Y.-K. Sun and D. Aurbach, *ACS Appl. Mater. Interfaces*, 2015, **7**, 16590–16600.

116 M. Saito, S. Yamada, T. Fujinami, S. Kosaka, Y. Tachikawa, K. Ito and Y. Kubo, *ECS Trans.*, 2017, **75**, 53–58.

117 D. Sharon, D. Hirsberg, M. Salama, M. Afri, A. A. Frimer, M. Noked, W. Kwak, Y.-K. Sun and D. Aurbach, *ACS Appl. Mater. Interfaces*, 2016, **8**, 5300–5307.

118 S. Wu, K. Zhu, J. Tang, K. Liao, S. Bai, J. Yi, Y. Yamauchi, M. Ishida and H. Zhou, *Energy Environ. Sci.*, 2016, **9**, 3262–3271.

119 H.-M. Kwon, M. L. Thomas, R. Tatara, A. Nakanishi, K. Dokko and M. Watanabe, *Chem. Lett.*, 2017, **46**, 573–576.

120 M. Saito, T. Fujinami, S. Yamada, T. Ishikawa, H. Otsuka, K. Ito and Y. Kubo, *J. Electrochem. Soc.*, 2017, **164**, A2872–A2880.

121 D. Hirshberg, D. Sharon, E. De La Llave, M. Afri, A. A. Frimer, W.-J. Kwak, Y.-K. Sun and D. Aurbach, *ACS Appl. Mater. Interfaces*, 2017, **9**, 4352–4361.

122 H.-M. Kwon, M. L. Thomas, R. Tatara, Y. Oda, Y. Kobayashi, A. Nakanishi, K. Ueno, K. Dokko and M. Watanabe, *ACS Appl. Mater. Interfaces*, 2017, **9**, 6014–6021.

123 A. Chamaani, M. Safa, N. Chawla, M. Herndon and B. El-Zahab, *J. Electroanal. Chem.*, 2018, **815**, 143–150.

124 L. Carbone, P. T. Moro, M. Gobet, S. Munoz, M. Devany, S. G. Greenbaum and J. Hassoun, *ACS Appl. Mater. Interfaces*, 2018, **10**, 16367–16375.

125 Y. Wang, N.-C. Lai, Y.-R. Lu, Y. Zhou, C.-L. Dong and Y.-C. Lu, *Joule*, 2018, **2**, 2364–2380.

126 G. Horwitz, C. Rodríguez, M. Factorovich and H. R. Corti, *J. Phys. Chem. C*, 2019, **123**, 12081–12087.

127 M. Tang, J.-C. Chang, S. R. Kumar and S. J. Lue, *Energy*, 2019, **187**, 115926.

128 Y. Hayashi, S. Yamada, T. Ishikawa, Y. Takamuki, M. Sohmiya, H. Otsuska, K. Ito, Y. Kubo and M. Saito, *J. Electrochem. Soc.*, 2020, **167**, 020542.

129 G. Horwitz, E. J. Calvo, L. P. Méndez De Leo and E. de la Llave, *Phys. Chem. Chem. Phys.*, 2020, **22**, 16615–16623.

130 V. Marangon, C. Hernandez-Rentero, S. Levchenko, G. Bianchini, D. Spagnolo, A. Caballero, J. Morales and J. Hassoun, *ACS Appl. Energy Mater.*, 2020, **3**, 12263–12275.

131 B. Scrosati, J. Hassoun and Y.-K. Sun, *Energy Environ. Sci.*, 2011, **4**, 3287.

132 L. Goldie-Scot, <https://about.bnef.com/blog/behind-scenes-take-lithium-ion-battery-prices/>, BloombergNEF, March, 5, 2019.

133 D. J. Eyckens and L. C. Henderson, *Front. Chem.*, 2019, **7**, 263.

134 D. Morales, R. E. Ruther, J. Nanda and S. Greenbaum, *Electrochim. Acta*, 2019, **304**, 239–245.

135 L. Carbone, S. G. Greenbaum and J. Hassoun, *Sustainable Energy Fuels*, 2017, **1**, 228–247.



136 J. B. Robinson, K. Xi, R. V. Kumar, A. C. Ferrari, H. Au, M.-M. Titirici, A. Parra-Puerto, A. Kucernak, S. D. S. Fitch, N. Garcia-Araez, Z. L. Brown, M. Pasta, L. Furness, A. J. Kibler, D. A. Walsh, L. R. Johnson, C. Holc, G. N. Newton, N. R. Champness, F. Markoulidis, C. Crean, R. C. T. Slade, E. I. Andritsos, Q. Cai, S. Babar, T. Zhang, C. Lekakou, N. Kulkarni, A. J. E. Rettie, R. Jervis, M. Cornish, M. Marinescu, G. Offer, Z. Li, L. Bird, C. P. Grey, M. Chhowalla, D. Di Lecce, R. E. Owen, T. S. Miller, D. J. L. Brett, S. Liatard, D. Ainsworth and P. R. Shearing, *J. Phys.: Energy*, 2021, **3**, 031501.

137 W. Chen, T. Lei, C. Wu, M. Deng, C. Gong, K. Hu, Y. Ma, L. Dai, W. Lv, W. He, X. Liu, J. Xiong and C. Yan, *Adv. Energy Mater.*, 2018, **8**, 1702348.

138 N. Mahne, O. Fontaine, M. O. Thotiyil, M. Wilkening and S. A. Freunberger, *Chem. Sci.*, 2017, **8**, 6716–6729.

139 A. C. Luntz and B. D. McCloskey, *Chem. Rev.*, 2014, **114**, 11721–11750.

140 W. Xu, V. V. Viswanathan, D. Wang, S. A. Towne, J. Xiao, Z. Nie, D. Hu and J.-G. Zhang, *J. Power Sources*, 2011, **196**, 3894–3899.

141 D. Aurbach, B. D. McCloskey, L. F. Nazar and P. G. Bruce, *Nat. Energy*, 2016, **1**, 16128.

142 S. A. Freunberger, Y. Chen, F. Bardé, K. Takechi, F. Mizuno and P. G. Bruce, in *The Lithium Air Battery*, eds. N. Imanishi, A. C. Luntz and P. Bruce, Springer New York, New York, NY, 2014, pp. 23–58.

143 W.-J. Kwak, Rosy, D. Sharon, C. Xia, H. Kim, L. R. Johnson, P. G. Bruce, L. F. Nazar, Y.-K. Sun, A. A. Frimer, M. Noked, S. A. Freunberger and D. Aurbach, *Chem. Rev.*, 2020, **120**, 6626–6683.

144 H.-G. Jung, J. Hassoun, J.-B. Park, Y.-K. Sun and B. Scrosati, *Nat. Chem.*, 2012, **4**, 579–585.

